CTH-NT-314

THESIS FOR THE DEGREE OF DOCTOR OF PHILOSOPHY

Radiation Detection Techniques for the Enhancement of Nuclear Safety

PETTY CARTEMO

Nuclear Engineering
Department of Applied Physics
Chalmers University of Technology
S-412 96 Göteborg, Sweden 2015

Radiation Detection Techniques for the Enhancement of Nuclear Safety
PETTY CARTEMO
ISBN 978-91-7597-244-2

Doktorsavhandling vid Chalmers tekniska högskola
Ny serie nr 3925
ISSN 0346-718X

Nuclear Engineering
Department of Applied Physics
Chalmers University of Technology
S-412 96 Göteborg
Sweden
Telephone +46 (0)31 772 1000
Fax +46 (0)31 772 3872

Cover: Visualization of the main topics covered by the thesis in form of the ionizing radiation sign.

Chalmers Reproservice
Göteborg, Sweden 2015

"Radiation Detection Techniques for the Enhancement of Nuclear Safety"
PETTY CARTEMO

Nuclear Engineering
Department of Applied Physics
Chalmers University of Technology

ABSTRACT
The hazard originating from the use of nuclear materials in various areas of the society necessitates a number of experimental techniques for controlling and increasing the safety connected to radioactive substances.
The following thesis is divided into two parts, representing different aspects to the detection of radiation effects.

The first part aims at investigating radiation-induced material damage of steel alloys that may potentially be used in future Generation IV systems. Concepts like the LFR or SFR will operate under higher temperature and radiation levels than in present LWR and detailed knowledge on the material integrity under high level conditions is important for the performance of the major safety barrier and thus the safety of a nuclear power plant. Ion-irradiation is used to simulate neutron-induced damage and the microstructure of the samples is investigated with the help of Positron Annihilation Lifetime Spectroscopy with the Chalmers Pulsed Positron Beam. A study regarding problems and challenges of ion-irradiation experiments is included. Additionally, depth profiling for the calibration of the measurement setup is performed.

The second part aims at experimental and computational methods for purposes of Nuclear Safeguards and Emergency Preparedness, respectively. The chapter on safeguards measurements treats two of the major issues within the field, namely spent fuel and nuclear forensics. Firstly, an independent method for investigations of the boron content in a PWR spent fuel pool is presented, demonstrating how liquid scintillator detectors can be applied for estimations of the relative amount of neutrons absorbed in H and B. Secondly, HPGe measurements on strong Am-sources are performed for a qualitative analysis of inherent impurities to be used as signatures for the identification of unknown sources, helpful to forensic investigations.
The chapter on emergency preparedness summarizes the computational work that was performed for simulations of source distributions in human phantoms. The IRINA voxel phantom is presented and Monte Carlo simulations for comparisons to the IGOR voxel phantom and the ICRP reference adult male voxel phantom are made for different distributions of Co and La in the human body.

Keywords: radiation-induced material damage; positron lifetime; pulsed beam; depth profiling; nuclear safeguards; orphan sources; Monte Carlo; voxel phantom; whole body counting

List of Appended Papers

PAPER I

P. Cartemo and A. Nordlund, "Depth profiling with the Chalmers pulsed positron beam"

International Journal of Nuclear Energy Science and Technology, Vol. 8 (2), 106-115 (2014)

PAPER II

P. Cartemo, A. Nordlund and M. Hernández-Mayoral, "Final report for GETMAT/WP4-4.3: Modeling oriented experiments in FeCr alloys - Positron lifetime measurements of irradiated FeCr alloy samples"

results published in the final group report: Hernández-Mayoral, M. et. al, "GETMAT D4.7 - Microstructure and microchemistry characterisation of ion-irradiated FeCr alloys (concentration, dose and temperature effect): TEM, PAS, APT and Synchrotron techniques" (2013)

PAPER III

P. Cartemo and A. Nordlund "Positron annihilation lifetime spectrometry for analyzing the impact of experimental parameters when emulating neutron damage with ion-irradiation experiments"

submitted to Journal of Nuclear Materials (2015)

PAPER IV

D. Chernikova, K. Axell, I. Pázsit, A. Nordlund, P. Cartemo, "Testing a direct method for evaluating the concentration of boron in a fuel pool using scintillation detectors, and a 252Cf and an 241Am-Be source"

Proceedings of the ESARDA 35th Annual Meeting 2013, Brugge, Belgium, May 28-30 (2013)

PAPER V

A. Vesterlund, D. Chernikova, P. Cartemo, K. Axell, A. Nordlund, G. Skarnemark, C. Ekberg, H. Ramebäck, "Characterization of strong 241Am sources"

Applied Radiation and Isotopes, Vol. 99, 162-167 (2015)

PAPER VI

P. Cartemo, J. Nilsson, A. Nordlund and M. Isaksson, "Letter to the editor"

published online in Radiation Protection Dosimetry Advance Access (2015)

PAPER VII

P. Cartemo, J. Nilsson, A. Nordlund and M. Isaksson, ”Building a generic voxel phantom of IRINA for Monte Carlo simulations”

Nordic Nuclear Safety Research, report number NKS-323 (2014)

PAPER VIII

P. Cartemo, J. Nilsson, M. Isaksson and A. Nordlund, ”Comparison of computational phantoms and investigation of the effect of biodistribution on activity estimations”

accepted for publication in Radiation Protection Dosimetry (2015)

Author's contributions

PAPER I
The author planned the experiment, performed all measurements and data analysis (including figures and tables) and wrote the manuscript.

PAPER II
The author performed all measurements and data analysis (including figures and tables) and co-wrote the manuscript.

PAPER III
The author performed all measurements and data analysis (including figures and tables) and wrote the manuscript.

PAPER IV
The author performed parts of the measurements and data analysis.

PAPER V
The author studied interaction probabilities for the evaluation of measurement data.

PAPER VI
The author wrote the manuscript.

PAPER VII
The author developed and programmed the algorithm and wrote the manuscript.

PAPER VIII
The author planned parts of the computational study, performed the analysis of all simulation data (including figures and tables) and wrote the manuscript.

Related work not included in this thesis

P. Cartemo, ”Measurements of Positron Penetration Depth at Low Energies with a Pulsed Beam”
Proceedings of the IYNC-2010, Cape Town, South Africa, July 12-18 (2010)

P. Cartemo and A. Nordlund, ”Status reports 2009, 2010 and 2011 for GETMAT/ WP4-4.3: Modeling oriented experiments in Fe and FeCr alloys - Positron lifetime measurements of irradiated FeCr alloy”
unpublished internal reports to the members of GETMAT/WP4 (task 4.3), December 2009, 2010 and 2011

A. Nordlund and P. Cartemo, ”GENIUS (WP2) progress report: Positron lifetime measurements of irradiated Fe and FeCr alloy samples”
unpublished internal report to the coordinators of GENIUS, December 2011

P. Cartemo and A. Nordlund, ”GENIUS (WP2) final report: Positron lifetime measurements of irradiated Fe and FeCr alloy samples”
unpublished internal report to the coordinators of GENIUS, December 2013

P. Cartemo, A. Nordlund, D. Chernikova and W. Ziguan ”Sensitivity of the neutronic design of an Accelerator-Driven System to the anisotropy of yield of the neutron generator and variation of nuclear data libraries”
Proceedings of the ESARDA 35th Annual Meeting 2013, Brugge, Belgium, May 28-30 (2013)

I. Pázsit, C. Montalvo, H. Nylén, T. Andersson, A. Hernández-Solís and P. B. Cartemo, ”Developments in core barrel motion monitoring and applications to the Ringhals PWR units”
accepted for publication in Nuclear Science and Engineering (2015)

C. Grah, K. Afanaciev, P. Bernitt et. al, ”Radiation hard sensors for the beam calorimeter of the ILC”
Nuclear Science Symposium Conference Record, Vol. 3, 2281-2284 (2007)

K. Afanaciev, M. Bergholz, P. Bernitt et. al, ”Investigation of the radiation hardness of GaAs sensors in an electron beam”
Journal of Instrumentation, Vol. 7 (11) (2012)

CONTENTS

Abstract i
List of Appended Papers iii

Foreword **1**
Radiation 1

I Material Sciences **5**

1 Sustainability through Nuclear?! **7**

2 Radiation Damage **11**
2.1 Damage Correlation 14
2.2 Simulating Neutron Damage with Heavy Ions 16

3 Positrons **19**
3.1 History and Common Use 19
3.2 Positron Interactions with Matter 21
3.2.1 Positron Lifetime 22
3.3 Positron Experiments for the Study of Solids 25
3.3.1 Doppler Broadening Spectroscopy 25
3.3.2 Slow Positron Beam 26
3.3.3 Lifetime Extraction 28
3.4 Depth Profiling 30
3.4.1 Au-layered Silica 30
3.4.2 Monte Carlo Simulations 30

3.4.3 Lifetime Measurements . . . 32
3.4.4 Conclusions . . . 33

4 Steel Alloys **35**
4.1 GETMAT . . . 35
4.1.1 FeCr Specimen . . . 36
4.1.2 Measurements . . . 38
4.1.3 Defect Analysis . . . 39
4.1.4 The Importance of Irradiation Parameters . . . 41
4.2 GENIUS . . . 43
4.2.1 FeCrAl Specimen . . . 43
4.2.2 Results and Conclusions . . . 44
4.2.3 Conclusions . . . 44

II Nuclear Safeguards and Emergency Preparedness **47**

5 Introduction **49**
5.1 On the Safety of Radioactive Materials and the NPT . . . 49
5.2 Emergency Preparedness - what if...? . . . 51

6 Radiation Detection **53**
6.1 Gas-filled Detectors . . . 54
6.2 Scintillator Detectors . . . 55
6.3 Semiconductor Diode Detectors . . . 56

7 Nuclear Safeguards Measurements **57**
7.1 Spent Fuel . . . 57
7.1.1 Novel experiments for estimating the amount of B in water 57
7.2 Nuclear Forensics . . . 59
7.2.1 Characterization of strong Am-241 sources . . . 60

8 Simulating Source Distributions in Humans **63**
8.1 The IRINA phantom . . . 63
8.1.1 Technical Data . . . 63
8.1.2 The IRINA voxel phantom . . . 65
8.2 Comparison of Phantoms . . . 65
8.2.1 Simulations . . . 66
8.2.2 IRINA vs. IGOR . . . 66
8.2.3 IRINA vs. ICRP . . . 68
8.2.4 Effect of biodistribution on WBC calibration . . . 69

9 Summary **73**
9.1 Part I - Material Research 73
9.2 Part II - Nuclear Safeguards and Emergency Preparedness 74
9.3 Outlook 75

Acknowledgements **77**

References **79**

PAPERS I-VIII **88**

Foreword

Radiation - out of control or under control?

The following thesis consists of three main topics, divided into two parts, that all deal with certain aspects of radiation. These three topics are Material Sciences (Part I), Nuclear Safeguards and Emergency Preparedness (Part II).

Safeguards is a field of research that partly concentrates on detector technologies to help prevent the unauthorized spreading of fissile material. Thus, safeguards deal with the *control of radiation*! In order for radiation to be *under control*, it is necessary to understand the behavior of a material upon irradiation and whether its radiation resistance can be ensured despite certain property changes. If handled carelessly or if protective materials deteriorate, radiating sources can get *out of control*. Radiation protection and emergency preparedness measures are then needed to minimize the effects of environmental or internal contamination.

Radiation

In physics, radiation is defined as the emission of energy as electromagnetic waves or subatomic particles [1]. The discovery of ionizing radiation by H. Becquerel (1852 - 1908) in 1896 did not only lead to the 1903 Physics Nobel Prize in Physics [2] but to great developments in science as well as knowledge helping to understand mysteries of our universe.

Low-energetic light, i.e. all wavelengths beyond the ultra-violet range, is considered to be non-ionizing and interaction with matter involves mainly thermal processes. It is the category of ionizing radiation that often spuriously creates fear and confusion. The different types of directly or indirectly ionizing radiation are, to varying extent, crucial for the topics presented in this thesis and are listed as:

- alpha radiation (α) and other heavy charged particles;
- beta radiation (β), especially positrons (β^+);
- gamma radiation (γ);
- neutron radiation (n).

Subatomic particles and heavy ions deposit their energy primarily by means of Coulomb interactions and collisions until finally absorbed by the interacting medium. The comparatively short range of particle radiation is, except for the case of neutrons, determined by each particle's mass and charge. Radiation in the form of high-energetic electromagnetic waves (γ) deposits its energy in a characteristic manner and over comparatively long distances. Neutrons on the other hand have no charge and interact with matter primarily through collisions with other nuclei. The range of neutrons in matter is long which is due to their low scattering probability at high energies.

Radioactivity is defined as the ability of an atom to emit radiation and is often observed in connection with the decay of an unstable isotope to a more favorable state. Unstable nuclei disintegrate by β-emission or electron capture; very heavy ones emit α-particles or may even undergo spontaneous fission. Principally every decay leaves an excited atom behind which in turn decays to the ground state by γ-emission. The strength of a radioactive source, i.e. its activity, is described by the amount of disintegrations per second. It is measured in Bq and decreases exponentially with time:

$$A(t) = A_0 \cdot \exp^{-\lambda t} \tag{1}$$

Every possible decay is characterized by an isotope-specific decay constant λ from which it is possible to calculate the half-life $T_{1/2}$. The decay path, its respective half-life and certain characteristic energies of all known isotopes are summarized in the "Chart of Nuclides", cf. Fig. 5.1 [3].

Radiation in the form of background radiation is present everywhere! On earth, there are principally two sources contributing to background exposure:

- Natural radioactivity originates from space, soil and living organisms that accumulate small quantities of radioactive isotopes. Between 50 and 100% of the annual background is considered to come from natural sources where significant variations are caused by altitude and geology.
- The remaining sources to background radiation are man-made and result mainly from X-ray technology and other medical applications. Less than 0.1% of all man-made sources are considered to originate from nuclear power and atomic bomb testing where differences may occur due to the near of nuclear sites or contaminated areas [4].

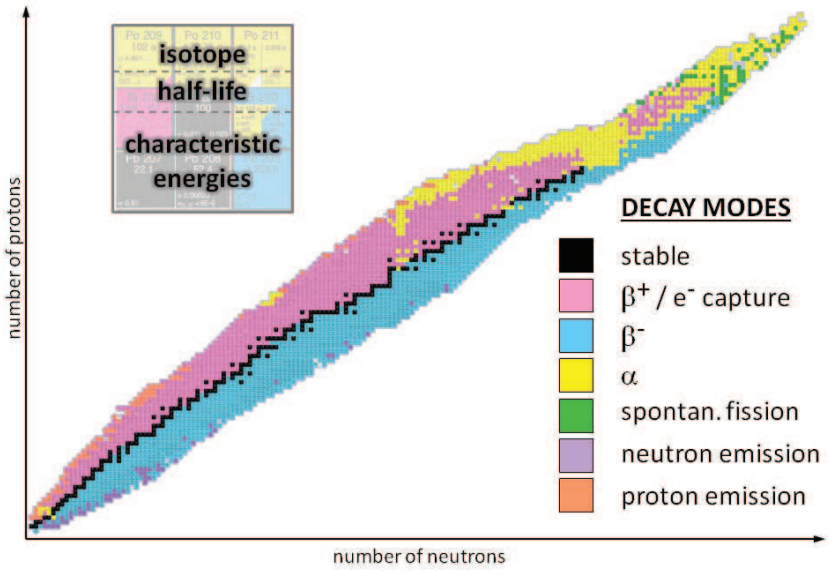

Figure 1: The nuclide chart contains several decay characteristics for all known isotopes. The color of each tile indicates the type of decay for the corresponding nuclide as well as its specific half-life and relevant energies. [3]

Exposure to elevated levels of ionizing radiation, whether natural or artificial, may pose a significant health risk to living organisms which is why radiation safety has become a major concern of nuclear technologies like power production, waste management and medical applications. While activity measures the strength of a given radioactive source, the concept of dose attempts to relate a source's physical properties to radiation effects in the interacting medium. The absorbed dose, measured in Gy, is the amount of energy deposited by any kind of radiation per unit mass. The equivalent dose, given in Sv, accounts for the biological effect of absorbed dose. This is done by multiplication with a weighing factor which changes with regard to the kind of radiation due to differing interaction characteristics. Lastly, an organ-specific tissue weighing factor is necessary for defining the effective dose, also in Sv, absorbed by living organisms [5].

The basic principles of radiation protection strive towards limiting the effects of the effective dose by shielding, distance and duration. Shielding procedures may vary for different types of radiation since energy deposition mechanisms depend on radiation-specific interaction probabilities. The dose received from a radioactive source follows the inverse-square law by distance and safety measures often include remote handling. Finally, the duration of exposure to radiation should be kept at a minimum and with respect to the principle of "ALARA" (As Low As Reasonably Achievable). Even if the human senses are not sensitive to ionizing radiation, it is generally very easy to detect any kind of nuclear radiation with the help of detectors.

Part I

Material Sciences

CHAPTER

1

Sustainability through Nuclear?!

Our planet has always been and will always be a place of great change. Just that about 250 years ago, with the start of the industrial revolution, society and science developed in a way not seen before. Since 1800, the world population has quickly grown from approximately 1 to more than 7 billion people as of today and this development does not yet seem to slow down significantly [6, 7].

Cities are growing, transport is fast and far, politics and economy are worldwide and so are industries and agriculture. In the Western World, daily demands such as clean water, regular and diverse food supply, hygienic needs and proper health, are out of doubt for most people even though those things require lots of resources behind the scenes. But even more luxurious parts of daily life have become a basic need!
Do we question the use of electric light and the need for a refrigerator? What about heating or cooling the places we live and work at? Could we honestly be without remote communication and broadcasted information?

Our dependency on energy in the form of electricity necessitates large-scale production and hand-in-hand with power plant development, materials for safe construction and reliable maintenance, all under consideration of social and environmental aspects, have to be developed to secure our daily needs.

Life no longer is a matter of survival only. Instead, nature struggles with the consequences of our acting and eventually will "pay back" somehow. Since a few decades back, climate researchers predict a parallel between increased human activity and greenhouse gas emissions that might accelerate climate change [8, 9]. An obvious cause for elevated levels of carbon dioxide and methane in the atmosphere is said to arise from combustion processes such as used for electricity

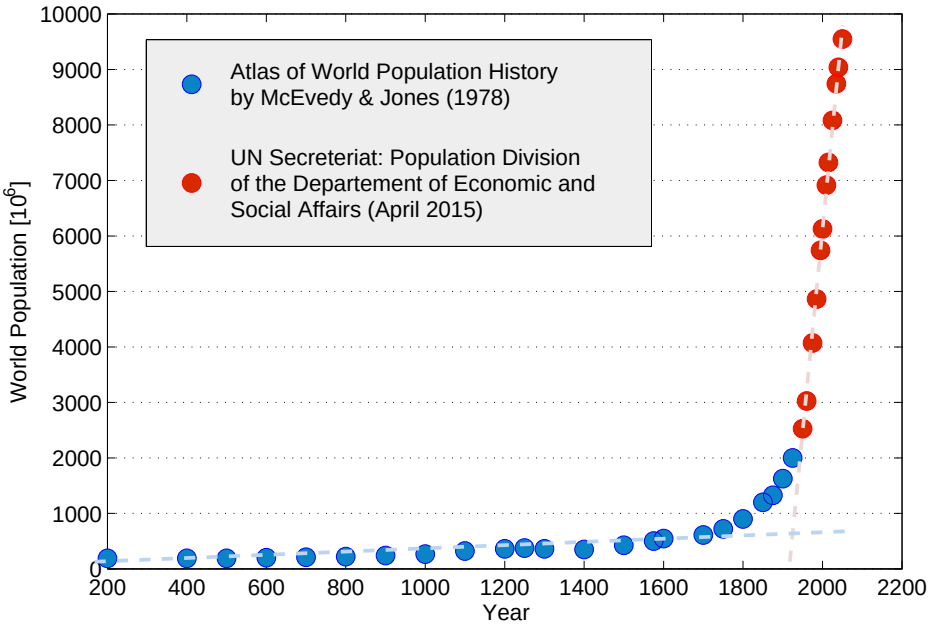

Figure 1.1: Diagram of the population growth throughout the last two millennia. According to the UN Secretariat, the world population continues to increase until 2050 at least. [6,7]

generation. For instance, countries like India, China and South Africa power themselves by 70, 80 and 90% from coal combustion, respectively [10]. It is predicted that the world population will continue to grow and with it the need for electric energy and if living standards shall continue to improve, especially in developing countries, decreasing the supply of electricity is not an option. If climate change really is due to human activity there is no time to lose and the amount of greenhouse gas emissions has to be reduced as soon as possible.

Apart from a number of ethical issues related to climate change, electricity and population, the energy sector may partly find a solution to the problems in the use of smart technology [11,12]. This, on the other hand, depends strongly on social awareness, personal engagement, long-term politics and investments. It is absolutely necessary to get away from fossil fuels for the production of electricity but neither hydro, wind or solar power are optimal solutions everywhere on the planet. Here, nuclear power could play a key role!

Present nuclear reactors have a high power density and are reliable and safe in relation to risks from other large-scale industrial facilities. Also, life cycle emissions are minimal compared to other energy sources and need to be taken into account when discussing electricity production and its impact on the climate.

However, the world's nuclear fleet is turning old and most existing units face their shut-down in the next 10-30 years [13]. Building and maintaining nuclear power plants is expensive and complicated in terms of legal and political aspects. The public acceptance for the nuclear industry is generally very low and even though we have been producing large amounts of nuclear waste for more than 50 years the question on how to deal with it is not yet solved. But several countries have once again realized the benefits of nuclear power and are building or planning new units of the third generation of power reactors.

Furthermore, research is going on towards a new generation of fission reactors. Today, the six reactor concepts appointed by the Generation IV International Forum (GIF) only exist on the drawing board [14, 15]. They are designed to be inherently safe and the nuclear fuel is supposed to be used in a more efficient manner, reducing the amount of waste to be taken care of. To meet these features as well as proliferation resistance, light water does no longer act as moderator and/or coolant. Ahead of that, researchers envision an all-inclusive plant that produces fuel, generates electricity and handles waste all at once.

Most of the proposed designs are considered to be used as breeding reactors, thus exhibiting a fast neutron spectrum. This in turn leads to much higher radiation doses than what is known from commercial Generation 2 and 3/3+ reactors. Furthermore, the operation temperature is substantially increased in most cases and chemical interactions between materials within the core have to be taken into consideration. It will take several years for commercial Generation IV systems to be put in operation safely since many issues still have to be solved. In the following chapters, aspects regarding possible materials for large, structural core components that will be subject to high irradiation and temperature are touched upon.

CHAPTER

2

Radiation Damage

The environment that is found in any nuclear power reactor is characterized by high temperatures and strong radiation, all in combination with mechanical forces and chemical reactions of various kinds. The magnitudes of the above clearly depend on where in the reactor observations are made but all are interdependent and put high demands on the materials used. Research regarding the effects of radiation on condensed matter is an important topic within nuclear material science and helps to guarantee safe reactor operation over long periods of time. The fission process releases enormous amounts of energy and results in particle fluxes of α, β, γ, massive ions and neutrons. These fluxes move through different parts of the reactor in form of radiation and interact with the materials in various ways. The interaction mechanisms may differ strongly for each particle category and in the field of reactor material research, lattice damage due to neutrons presents one of the most important subjects [16,17].

The steel alloys studied within this thesis are probable candidates for structural components and may be used for constructing the reactor pressure vessel and core internals for future reactor systems. In contemporary light water reactors (LWR), the neutrons are thermalized and reflected back into the core in an efficient manner and the flux to the walls of the pressure vessel remains low enough to guarantee a safe operational reactor lifetime of 40 years and longer. Breeder or GenIV reactors require higher neutron energies and fluxes to reach criticality which in turn has an effect on material properties with respect to radiation resistance. Improved vessel materials have to be developed since doses are expected to be as much as approximately 10 times higher than in thermal reactors [18–20].

One can consider four major categories when discussing the effects of radiation on matter [21]. Effects such as impurity production and atom displacement are the most relevant categories for reactor material research where severe structural changes of core components have the ability to adventure nuclear safety. The remaining categories - ionization and heat deposition - do not contribute significantly to the study of metals and alloys in nuclear reactors but play a very important role when discussing interaction mechanisms between radiation and living tissue or electro-sensitive materials such as semi-conductors and polymers.

The ability of ionization to break chemical bonds increases with the decreasing strength of a molecular formation which is why ionization is a substantial aspect of radiation damage to biological organisms. The heat produced in one fission event is deposited within the fuel by as much as 84% and leads to very localized thermal effects. Thus, radiative heat deposition does not contribute significantly to the damage produced in core internals other than the fuel itself. Fission fragments and fission gases like He (α particles) or H (protons) act on a short range and cause atom displacements as well as direct impurities merely in the vicinity of their point of creation, i.e. the fuel.

The effects of neutron radiation though can be seen throughout all parts of the reactor and the availability of strong neutron fluxes contributes to material research in a unique way. The neutron energy spreads over a wide spectrum and due to the absence of electric charge, neutrons travel long distances despite their high mass. They interact by scattering on other nuclei and can only be stopped by absorption.

Primarily, ballistic collisions between energetic neutrons and nuclei are elastic and the neutron energy after one scattering event, E', can be calculated by

$$E' = \frac{1}{2}E \cdot [(1+\alpha) + (1-\alpha) \cdot \cos(\theta)] \tag{2.1}$$

where E is the energy prior to collision with the scattering angle θ and α is defined as

$$\alpha = \left(\frac{(A-1)}{(A+1)}\right)^2 \tag{2.2}$$

with A being the atomic mass number of the scattered nucleus [22].

The maximum fractional energy loss after one collision equals $(1-\alpha)$ and is only dependent on the mass of the scattering center. The average logarithmic energy decrement per collision is defined as

$$\xi = 1 - \frac{(A-1)^2}{2A} \cdot \ln\left(\frac{A+1}{A-1}\right) \tag{2.3}$$

and decreases as A increases [23]. It turns out that the average number of collisions for equal amounts of energy loss is directly proportional to the mass of the scattered nucleus, cf. Fig. 2.1.

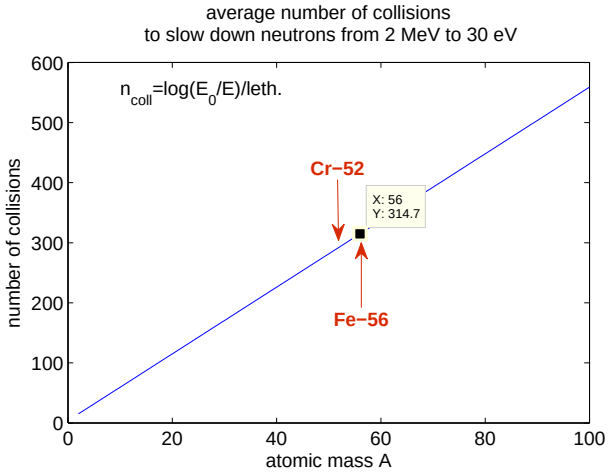

Figure 2.1: Average number of collisions as a function of atomic mass for the slowing down of neutrons from 2 MeV to 30 eV.

Considering that neutrons in a nuclear reactor exhibit a wide energy spectrum, it becomes obvious that large amounts of energy may be transferred in subsequent collisions with other nuclei. This is taken advantage of when moderating neutrons - a necessary process for sustaining the fission chain reaction - but for other materials that encounter neutron radiation, it puts great demands on material properties and their performance.

The effects of radiation damage due to atom displacement are related to three major categories of microscopic point defects: vacancies, interstitials and dislocations. A neutron that escapes the reactor core eventually interacts with the surrounding pressure vessel by colliding with nuclei of the atomic lattice. If the energy transferred in one collision exceeds a certain threshold energy $E_d \leq E - E'$, the neutron causes atom displacement of the struck lattice atom which then is entitled Primary Knock-on Atom (PKA) [24, 25]. When a PKA leaves its initial position, a vacancy is left behind, i.e. an empty space within the lattice. When it comes to rest, it is terminated and turns into an interstitial atom. Vacancies and interstitials always come in pairs and one such formation is often related to as Frenkel pair. If instead the regular structure of a crystal-arrangement is deformed, layers of several misplaced atoms are formed. These are considered as dislocations and are often formed upon mechanical work on the material.

The displacement energy E_d for steels and alloys, such as used for the reactor pressure vessel, is around 25 to 40 eV and one fast neutron ($E_{kin} \sim 1$ MeV) has the ability to create several hundred PKAs on its path through the material. If the energy of such a PKA is sufficiently large, it may create secondary and tertiary knock-on atoms leading to displacement cascades [24]. Apart from that one neutron has the ability to create numerous Frenkel pairs, vacancies and

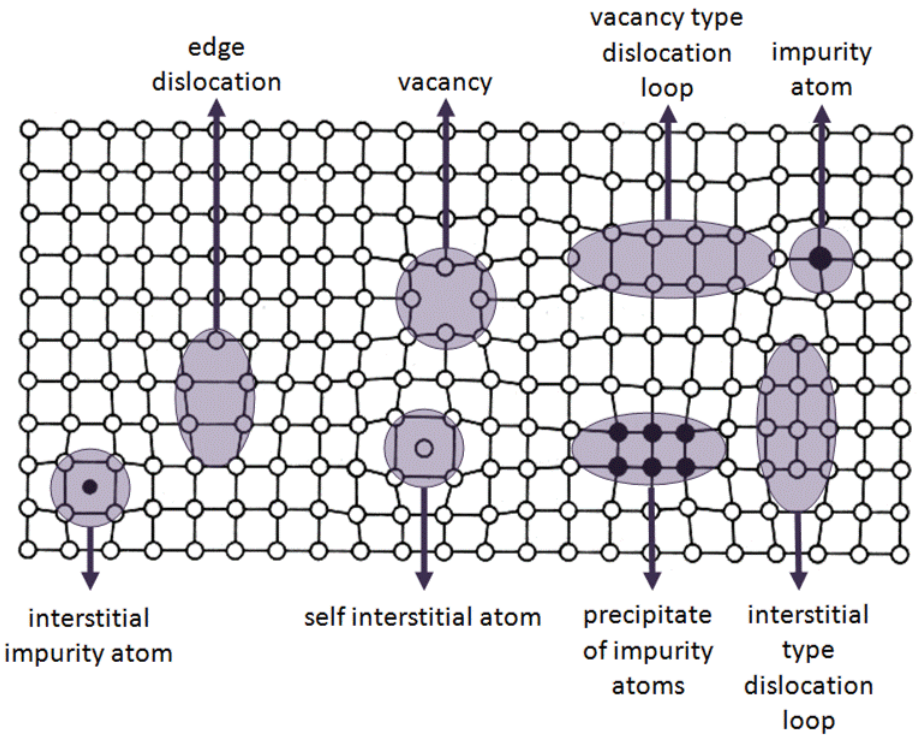

Figure 2.2: Illustration of typical microscopic lattice defects [26].

interstitials have individual kinematic properties that allow for clustering and recombination. The migration of point defects and their aggregates is temperature-dependent and creates macroscopic damage such as depletion zones, voids, cavities and replacement collisions [27].

A neutron may finally be terminated when absorbed by a lattice atom which in cases may even lead to the activation of the nucleus[1]. The absorption of the neutron creates a direct impurity which affects the lattice structure and material characteristics due to changes of the atomic composition.

2.1 Damage Correlation

In order to guarantee a material's performance and integrity in a nuclear environment, it is important to understand the development of defects upon irradiation and temperature since long-time exposure can lead to serious material failure due to effects like swelling, creep, embrittlement or cracking. There is a number of parameters that are used to correlate these types of macroscopic damage to irradiation characteristics such as radiation type and energy, particle flux,

[1] Activation is the creation of a radioactive isotope that moves towards a stable state through a chain of decays

temperature and initial microstructure [28,29].

The most common parameter that tries to relate radiation dose to the damage caused by it, is the unit dpa which is the average number of displacements per atom. The concept of dpa is regularly applied to limit operational lifetimes of different reactor components, even if damage correlation is far more complex than only by the number of atoms displaced from their initial lattice site.

The amount of dpa cannot be measured directly and has to be calculated by numerical and/or analytical methods. Tools, that are commonly applied to quantify the damage achieved by varying sources of radiation, follow random particle trajectories individually so that numerical integration or probability analysis is performed by Monte Carlo calculations. One widely-used program package for research related to ion implantation is SRIM (Stopping and Range of Ions in Matter) [30,31]. The "TRansport of Ions in Matter" is simulated by the sub-program TRIM and is the most comprehensive part of SRIM. It includes basic physical models on material damage that can be associated to primary mechanisms of energy loss and any source of radiation (neutrons, ions, α, β, γ) can be defined as projectile. In context with this thesis, SRIM was used as a tool for estimating the range of Fe-ions in FeCr. However, phenomena related to the mobility of individual defects and clusters or the crystalline structure of the target material are not taken into account by the code. Instead, MD (molecular dynamics) simulations in combination with analytical solutions to the theory of atom displacement may help to understand defect behavior in a detailed, more realistic manner [32].

The number of atom displacements during a certain period of irradiation, t, can be calculated according to [24,27]

$$dpa = \frac{R_d \cdot t}{N} \tag{2.4}$$

Taking neutron irradiation as an example, the displacement rate, R_d, is proportional to the number of target atoms, N, with its dependance on neutron energy, E_n, being expressed through the displacement cross-section $\sigma_d(E_n)$ and the neutron flux $\phi(E_n)$:

$$R_d = N \cdot \sigma_d(E_n) \cdot \phi(E_n) \tag{2.5}$$

Since the displacement cross-section ideally accounts for the production of a PKA and the subsequent displacement cascade, it may describe a very complex interaction pattern so that simplifications to the elementary displacement theory become necessary in order to approximate the dose needed to achieve a certain level of damage. A model that is often referred to in the context of neutron irradiation is the one by Kinchin and Pease which primarily assumes that all displacements happen upon elastic two-body collisions. Then, R_d will be given as

$$R_d = N \cdot \lambda \frac{E_n}{4E_d} \sigma_{el}(E_n) \cdot \phi(E_n) \tag{2.6}$$

and the average number of atom displacements becomes

$$dpa = \lambda \frac{E_n}{4E_d} \sigma_{el} \cdot \phi(E_n) \cdot t \tag{2.7}$$

with the elastic scattering cross-section, σ_{el}, being weekly dependent on E_n and $\lambda = (4A/(1+A))^2$ (only valid for neutrons).

A number of modifications can be made to the K-P-model in order to relax some of its basic assumptions, including a more detailed treatment of the displacement cross-section. This, as well as a closer look at the basics of MD simulations, is out of the scope of this short overview. Damage correlation is very complex and theoretical as well as experimental approaches are under constant development.

2.2 Simulating Neutron Damage with Heavy Ions

Numerical calculations and in-depth simulations of neutron damage may reveal good knowledge on the principal behavior of defects for ideal materials but they lack experimental insights that are needed to prove theoretical models. The change of material characteristics and structures due to neutron radiation is a well studied topic. The experimental understanding is, however, limited by the availability of high yield neutron sources which is especially interesting in GenIV material research.

A large amount of samples for the study of neutron damage may be obtained from current LWRs but the thermal energy spectrum as well as comparatively low dose-rates and irradiation temperatures are drawbacks when trying to predict material behavior in a GenIV environment. Even if there are research reactors that offer a fast neutron spectrum, the problem of achieving high doses within a respectable time frame remains. Several examples from literature suggest that the dose-rate influences defect evolution to a greater extent than the total received dose [33–36]. Another major drawback of neutron irradiation is the activation of the material which makes sample handling enormously more difficult due to radiation protection routines.

A method that is applied to avoid disadvantageous properties of neutron irradiation experiments is to emulate neutron damage with the help of ions [37, 38]. There is a huge number of so-called accelerators that are widely used to create beams of heavy, charged particles. The diversity of former, present and future accelerators is reflected within the technology necessary to achieve ever increasing requirements on ion energy, research field and application. One of the most well-known accelerators of the present is the LHC (Large Hadron Collider) at CERN which uses ultrarelativistic protons for particle physics research.

Much simpler setups than the LHC are widely used to accelerate heavy ions to energies of magnitude MeV (maximum energy depends on ion mass). An ion

beam is easily adjusted by magnetic and electric fields so that the particle energy and thus penetration depth can be controlled in an efficient manner. The flux of ions can be tuned and very high irradiation doses may be achieved within a rather short time-frame.

While neutrons interact with matter more or less only by ballistic collisions (hard-sphere), charged particles interact with the atomic lattice of a material primarily on the base of Coulomb forces [39]. At high initial ion energies, the loss of kinetic energy is governed by inelastic scattering of the impinging ion with electrons of the medium and is referred to as electronic stopping. As the ion energy decreases, the probability for elastic scattering with nuclei of the material lattice, referred to as nuclear stopping, increases and allows for the production of recoil atoms. Recoils that receive a sufficient amount of energy are then displaced from their initial lattice position and may form displacement cascades and lattice defects similar to the processes described for neutron irradiation [40].

The charge-dependent energy loss mechanisms observed in ion-matter interactions result in a much shorter range of ions in matter than what neutrons have. But even if the created damage cascades may be of similar type and size, their inhomogeneous distribution in the near-surface region of the irradiated material give rise to microchemical and microstructural effects that may be different than if originating from neutrons [41].

The radiation-induced damage to a material lattice is usually quantified by dpa, i.e. the total number of "ballistic" displacements per atom, cf. eq.2.7. Describing damage in the case of charged particles, with the superior probability for Coulomb interactions, emphasizes the need to consider the distribution of recoil atoms resulting from any non-ballistic collision with the lattice.

The total number of primary recoil atoms (equivalent to PKA) created upon irradiation depends on the mass and energy of the impinging particle as well as the target material. As previously outlined, energy transfer in excess of E_d may lead to radiation damage in form of atom displacements. The fraction of recoils with energies larger than E_d is known as the primary recoil spectrum and the damage energy E_D that is produced in a recoil leads to the production of defects and subsequent cascades by atom displacements upon elastic collisions. The damage energy is a measure for the number of produced defects and by weighting the primary recoil spectrum with the damage energy produced by a recoil atom of particular energy, the distribution of damage over a certain energy range can be identified. The so-called "weighted average" recoil spectrum then gives the number of recoils that are produced by the incoming particle of energy E_i and is written as,

$$W(E_i, T) = \frac{1}{E_D(E_i)} \int_{E_d}^{T} \sigma(E_i, T') E_D(T') dT' \tag{2.8}$$

where

$$E_D(E_i) = \int_{E_d}^{T_{max}} \sigma(E_i, T') E_D(T') dT' \tag{2.9}$$

with $\sigma(E_i, T)$ being the energy transfer cross section for the production of a recoil with energy T, E_d the displacement threshold energy, T_{max} the maximum energy transferred in a collision, $E_D(E_i)$ the damage energy/number of defects produced by the incoming particle and $E_D(T)$ the damage energy/number of defects produced by the primary recoil of energy T [42,43].

Due to the structure of σ, there are two extremes to $W(E_i, T)$ for either Coulomb or hard-sphere interactions. While neutrons merely interact by ballistic collisions, protons lose almost all their energy in Coulomb interactions which tend to create many low-energetic PKAs. In the case of heavy ions, the Coulomb potential is screened and the repulsive force that is being "felt" between the interacting particles increases with ion mass, i.e. charge. The nuclear stopping power then exceeds the electronic stopping power which results in a hard-sphere type interaction. Consequently, irradiation with heavy-ions creates fewer PKAs than light-ions do but with higher energies. Subsequent displacement cascades lead to material damage in the form of large clusters that are, with increasing ion mass, regarded as comparable to neutron-induced damage [44].

To summarize, displacement mechanisms and interaction probabilities vary for different particles, dose rates and irradiation temperatures which makes it very difficult to compare radiation effects on matter. The dpa-unit tries to measure damage but is unfortunately not directly applicable for comparing different radiation sources since the created defects and their spatial distribution are not the same for all displacement cascades. Consequently, 1 dpa of heavy ion-irradiation has not the same effect as 1 dpa of neutron irradiation. The evolution of microscopic lattice defects into macroscopic damage contains detailed studies on migration, recombination or clustering and lead to phenomena observed in the form of embrittlement, cracking, phase transitions or swelling. However, the following piece of research only concentrates on a very little area of material sciences and does not aim at damage morphology. For a deeper analysis of radiation damage, the interested reader is advised to additional literature such as given by some of the references in this chapter [24,41,45].

CHAPTER

3 Positrons

"What sort of nonsense is this you're writing about in the papers?" [46]
comment by Ed McMillan on Carl D. Anderson's article "The apparent existence of easily deflectable positives", 1932 [47]

3.1 History and Common Use

In the early 1900's, physics was subject to change due to the upcoming of quantum mechanics. Throughout the following decades, great physicists formed modern theories leading to applications that once were impossible to imagine. Since 1928, theoretical considerations on quantum mechanics by Paul Dirac (1902 - 1984) proposed the existence of a positive electron charge [48,49] and in 1931 he published a paper [50], indirectly asking for experiments capable of validating the predicted anti-electron:

> "[*It*] would appear to us as a particle with a positive energy and a positive charge [...] Subsequent investigations, however, have shown that this particle necessarily has the same mass as an electron and also that, if it collides with an electron, the two will have a chance of annihilating one another [...] [*It*] would be a new kind of particle, unknown to experimental physics [...] We should not expect to find any of them in nature [...] but if they could be produced experimentally in high vacuum they would be [...] amenable to observation."

Finally in 1933, the editors of "Physical Review" received a paper that revolutionized particle physics since it proofed the existence of anti-matter [51]. Carl D. Anderson (1905 - 1991) summarized his measurements as such:

> "To date, out of a group of 1300 photographs of cosmic-ray tracks 15 of these show positive particles penetrating the lead, none of which can be ascribed to particles with a mass as large as that of a proton, thus establishing the existence of positive particles of unit charge and of mass small compared to that of a proton."

As one of the youngest Nobel Laureates ever, Anderson received the Nobel Prize in Physics in 1936 for his discovery of the positron [52]. Being the electron's anti-particle, the positron carries a positive unity-charge and interacts with matter in the same way as an electron does and, additionally, through annihilation. In the original experiment, positrons were created from highly-energetic γ-rays by pair-production but when Irène (1897 - 1956) and Frédéric (1900 - 1958) Joliot-Curie discovered "artificial radioactivity" in 1934, another source of positron radiation was found [53]. In a proton-rich, unstable nucleus one proton might be converted into a neutron while emitting a positron. This process is widely known as β^+-decay and presents a common and simple way of producing free positrons for experimental use.

$$p \rightarrow n + \beta^+ + \nu_e \tag{3.1}$$

The nuclide chart presents a huge amount of such sources but only few isotopes are of interest for positron applications. Within the field of oncology, PET (Positron Emission Tomography) is a widely used tool that exploits positrons for imaging purposes making it possible to locate tumors and even cancer metastases. Other medical fields involving positrons for both clinical needs and research are neuroimaging, cardiology and pharmacokinetics.

Besides studies involving living tissue, the interaction of positrons with condensed matter is interesting for the area of material research where special emphasis lies on defect studies and surface physics [54]. Related experiments that exploit positrons started to develop in the 1940s and today, there exists a number of several techniques that are, for example, capable of determining the size and/or concentration of positron-sensitive lattice defects present in condensed material or its surface thus allowing to study microscopic material properties. Common techniques involving positrons for non-destructive material testing are [55]:

- **P**ositron Annihilation-Induced **A**uger-**E**lectron **S**pectroscopy;
- **A**ngular **C**orrelation of **A**nnihilation **R**adiation;
- **D**oppler **B**roadening **S**pectroscopy;
- **P**ositron **A**nnihilation **L**ifetime **S**pectroscopy;
- **R**eemitted **P**ositron (or Positronium) **S**pectroscopy.

Transmission Positron Microscopy (TPM) and variations of it are other non-destructive testing devices with properties similar to TEM (Transmission Electron Microscopy). Furthermore, positrons are applied to study astrophysics or plasma phenomena and if the ILC (International Large Collider) becomes reality they may even help to confirm and deepen our knowledge on the Higgs boson.

3.2 Positron Interactions with Matter

The positron is the anti-particle to the electron. Both are elementary particles of equal mass and spin but carry opposite charge and magnetic moment and hence, positrons move in the opposite direction when subject to electric or magnetic fields. A free positron is stable in vacuum where confinement as well as motion control is achieved through electromagnetical fields.

Table 3.1: Basic properties of the electron and its anti-particle.

elementary particle	mass	spin	charge	magnetic moment
e^+	9.109e-31 kg	1/2	-1 e	-1 μ
e^-	9.109e-31 kg	1/2	+1 e	+1 μ

In general, positrons interact with condensed matter in the same way as electrons do. Highly-energetic particles mainly lose their energy by Coulomb interactions (elastic scattering) whereas excitation and ionization (inelastic scattering) are the dominant mechanisms of energy loss for particles with intermediate or low energy. Another channel for interaction occurs at very high particle energies in the form of bremsstrahlung. Every positron, regardless of energy, will face its termination through annihilation which is the most distinctive kind of interaction between anti-matter and matter.

The term ”an-nihil-ation” originates from the Latin word ”nihil” which translates to ”nothing” and ”annihilare” literally means ”to bring to nothing”. But thanks to A. Einstein (1879 - 1955) we know that nothing just disappears without a trace! In physics, the annihilation process is energy- and momentum-conserving and quantum numbers as well as charge of the involved particles add up to zero. The most favorable annihilation path for an electron-positron pair is the conversion into two photons of nearly equal wavelength. Here, the kinetic energy of the center-of-mass system is very close to zero and according to the rest mass of the positron/electron, each photon receives approximately 511 MeV. Triple-photon ejection is possible as well as Positronium formation under certain conditions. In accelerators, where energies up to several TeV are achieved, it is even possible to create heavy bosons from electron-positron collisions (such as W^+W^- pairs, Z and probably Higgs).

The typical interaction chain of a positron encountering condensed matter is characterized by a few material-specific parameters. A positron that reaches the surface of a solid may either be back-scattered into the surrounding medium or penetrate the material up to a certain depth (penetration depth). Immediately after entering the material, the positron is quickly brought into thermal equilibrium with its surroundings by subsequent scattering mechanisms. This process leads to an exponential implantation profile that can be approximated by the Makhovian depth distribution function [56, 57]:

$$p(z, E) = \frac{m \cdot z^{m-1}}{z_0^m} \exp\left[-\left(\frac{z}{z_0}\right)^m\right] \tag{3.2}$$

Here, z is the depth within the material as achieved by positrons of energy E and z_0 is calculated by

$$z_0 = \frac{AE^n}{\rho \cdot \Gamma(\frac{1}{m} + 1)} \tag{3.3}$$

n, m and A are material-dependent, empirical parameters, Γ is the gamma-function and ρ is the density.

The thermalization time is in the range of a few pico-seconds which means that the slowing down of positrons can be considered to be instantaneous. Once thermalized, positrons will diffuse through the material until they annihilate [58, 59]. While implantation is a rather straight forward process that mostly depends on initial particle energy, diffusion is primarily affected by temperature where particle motion is of random-walk character [60, 61]. If the initial positron energy is below 30 keV, positrons might back-diffuse to the surface which may lead to re-emission from the bulk material, positronium formation or surface annihilation. The theoretical value for the positron diffusion length is on the order of 100 nm and seems to be in contradiction to the Makhov model for low-energetic positrons and experimental measurements of positron deposition. Thus it is difficult to determine the total penetration depth and point of annihilation which creates one of the challenges within slow-positron measurements and depth profiling.

3.2.1 Positron Lifetime

One important positron parameter defines the time between the start of positron-matter-interaction and final annihilation - the positron annihilation lifetime. In metals, there are usually two different modes of annihilation that quantify the positron lifetime:

Free annihilation determines the mean or bulk lifetime of a positron in a well-defined, defect-free atomic lattice.

Trapped annihilation increases the lifetime due to positron trapping in lattice defects [62, 63]. Vacancies, dislocations and their aggregates change the atomic

lattice in a way as to attract positive charges and thus present traps for positrons that enter a defected solid.

The positron lifetime varies, depending on the type of material and presence of defect structures, between approximately 110 ps up to a couple of ns. Since the time scales covered by thermalization and diffusion are on the order of a few pico-seconds only, these processes do not affect the positron lifetime. A number of experimental and simulated values for the positron annihilation lifetime for some elements of the periodic system are presented in Figs. 3.1 and 3.2 [64]. Where applicable, lifetime values for free and for trapped annihilation can be found, i.e. bulk lifetime and mono-vacancy lifetime, respectively. A mono-vacancy terms the removal of an atom from the lattice site which reduces the electron density locally and creates an attractive potential for positively-charged particles. If a positron encounters such a region, it may be trapped within the defect in a way as to delay its annihilation with the surrounding valence electrons, generating at least one more lifetime component which is larger than the bulk lifetime.

A generally smaller delay is also found for defects created by dislocation structures where the electron density is reduced due to the misplacement of lattice sites. However, trapping is only possible if the dislocation-type defect is large enough since no atoms are removed from the lattice, cf. Fig. 2.2.

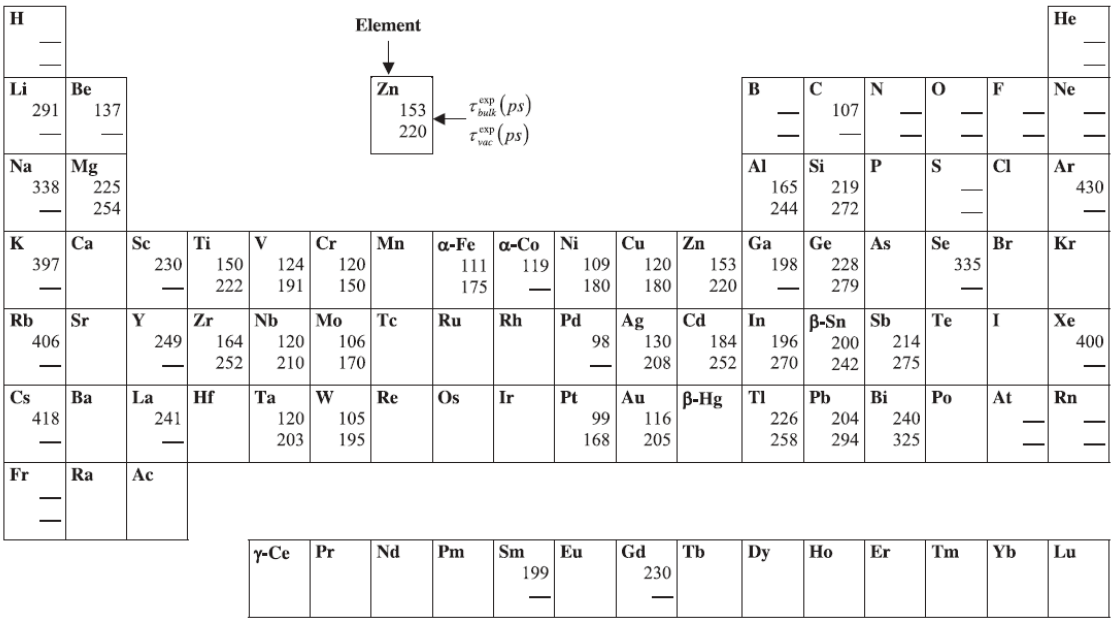

Figure 3.1: Experimental lifetime values for the bulk and mono-vacancy state for some elements. In each tile of the graphic, the top value represents the positron lifetime of the defect-free bulk material, τ_{bulk} and the bottom value is the lifetime for positron trapping in a mono-vacancy, $\tau_{vacancy}$. [64]

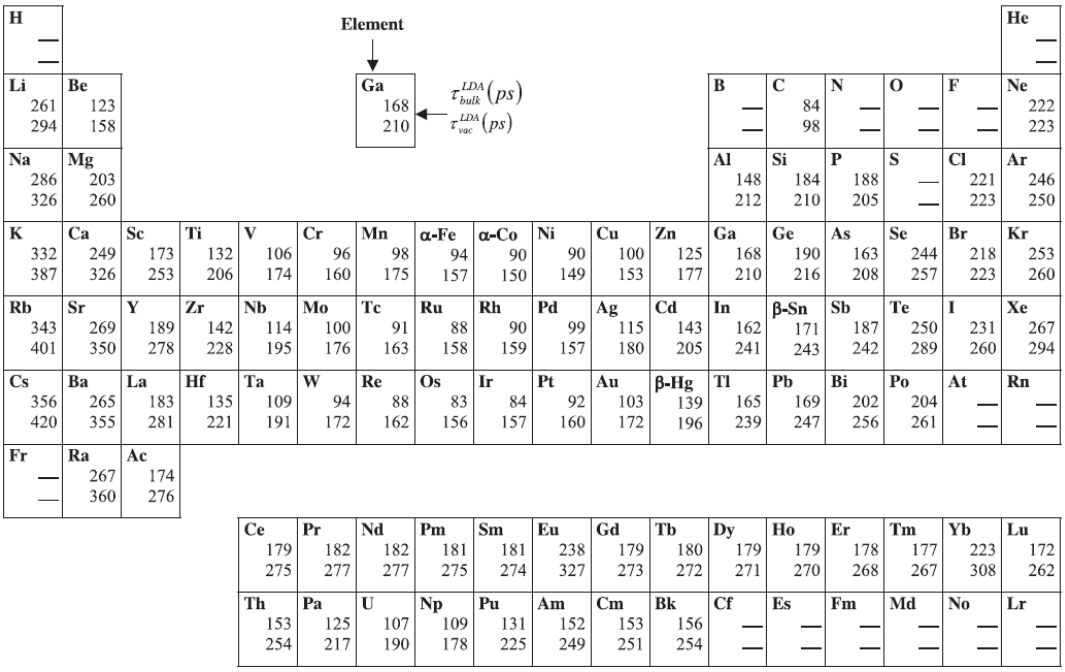

H — —																	He — —
Li 261 294	Be 123 158											B — —	C 84 98	N — —	O — —	F — —	Ne 222 223
Na 286 326	Mg 203 260											Al 148 212	Si 184 210	P 188 205	S — —	Cl 221 223	Ar 246 250
K 332 387	Ca 249 326	Sc 173 253	Ti 132 206	V 106 174	Cr 96 160	Mn 98 175	α-Fe 94 157	α-Co 90 150	Ni 90 149	Cu 100 153	Zn 125 177	Ga 168 210	Ge 190 216	As 163 208	Se 244 257	Br 218 223	Kr 253 260
Rb 343 401	Sr 269 350	Y 189 278	Zr 142 228	Nb 114 195	Mo 100 176	Tc 91 163	Ru 88 158	Rh 90 159	Pd 99 157	Ag 115 180	Cd 143 205	In 162 241	β-Sn 171 243	Sb 187 242	Te 250 289	I 231 260	Xe 267 294
Cs 356 420	Ba 265 355	La 183 281	Hf 135 221	Ta 109 191	W 94 172	Re 88 162	Os 83 156	Ir 84 157	Pt 92 160	Au 103 172	β-Hg 139 196	Tl 165 239	Pb 169 247	Bi 202 256	Po 204 261	At — —	Rn — —
Fr — —	Ra 267 360	Ac 174 276															

Ce 179 275	Pr 182 277	Nd 182 277	Pm 181 275	Sm 181 274	Eu 238 327	Gd 179 273	Tb 180 272	Dy 179 271	Ho 179 270	Er 178 268	Tm 177 267	Yb 223 308	Lu 172 262
Th 153 254	Pa 125 217	U 107 190	Np 109 178	Pu 131 225	Am 152 249	Cm 153 251	Bk 156 254	Cf — —	Es — —	Fm — —	Md — —	No — —	Lr — —

Figure 3.2: Calculated lifetime values for the bulk and mono-vacancy state for some elements. In each tile of the graphic, the top value represents the positron lifetime of the defect-free bulk material, τ_{bulk} and the bottom value is the lifetime for positron trapping in a mono-vacancy, $\tau_{vacancy}$. [64]

3.3 Positron Experiments for the Study of Solids

The simple way of producing positrons for experimental use is by a source with β^+-decay where an unstable isotope gains stability by positron emission. Candidates for β^+-decay are all isotopes above the stable line in the nuclide chart, cf. Fig. 1 but only those with a significant half-life are of practical use such as ^{22}Na, the most common isotope used within positron applications. Isolated positrons are easily controlled by electric and magnetic fields and their interaction with matter results in annihilation with electrons. Events happening prior to annihilation such as scattering and diffusion may differ significantly with respect to the aggregate of the target volume that can either be gaseous or solid, atomic or molecular. In the case of metallic lattices, this electron-positron annihilation usually renders two γ-rays of 511 keV energy each.

3.3.1 Doppler Broadening Spectroscopy

Conventional Doppler Broadening Spectroscopy (DBS) is a commonly applied technique for non-destructive testing with positrons [65]. Even if it has not directly been used for the purposes of this thesis, the basics of DBS are explained in the following.

In DBS, defect structures are characterized by the energy spread of the annihilation γ-rays. The energy of core electrons in a metal is distributed according to the Fermi-Dirac distribution, with the Fermi energy being on the order of 10 eV. The energy of a thermalized positron is less than 0.1 eV and thus the momentum of an electron-positron pair is mainly due to the contribution from the electron. This momentum distribution is then reflected in the energy of the emitted annihilation γ-rays in form of a Doppler shift that broadens the 511 keV peak in the energy spectrum, thus the name DBS [66].

The energy spread due to Doppler broadening is different for core and valence electrons. While core electrons are tightly bound to the nucleus, valence electrons sit in the outer shell of an atom and have a comparatively small momentum. This difference in momentum leads to a change in peak width and can be used to draw conclusions on the electron structure of the lattice which is altered by the presence of microscopic defects.

In the example of a mono-vacancy, one atom is removed from the lattice. Since the core electrons are tightly bound to the nucleus, they are most likely also removed from the lattice. The valence electrons on the other hand may remain in place. This leads to an overall higher fraction of valence electrons in the lattice when defects are present and thus, the probability for positrons annihilating with valence electrons increases. Since the total momentum of such an electron-positron pair is reduced, the Doppler broadening will be smaller than that for

positrons annihilating with core electrons. Conclusively, the measured energy spectrum is narrowed by defects that enhance positron trapping, i.e. vacancies and voids.

A typical DBS setup consists of one energy-sensitive detector such as a HPGe detector and a continuous positron emitting isotope that is then surrounded by the sample material (sandwich configuration). Coincidence measurements can be applied to reduce background and improve energy resolution, requiring an additional detector for the measurement of the second γ-particle from the annihilation process.

The recorded data is analyzed in terms of two parameters. The shape parameter S quantifies the narrowness of the Doppler-broadened energy spectrum in the proximity of the 511 keV peak and the wing parameter W measures the spectrum's sharpness in the high momentum region. Other than with a mono-energetic positron beam, it is difficult to gain defect-specific knowledge from DBS measurements because both S and W parameters change simultaneously with respect to defect type and concentration [55].

3.3.2 Slow Positron Beam

The positron annihilation lifetime, measures how long the positron survives after entering a material lattice and is inversely proportional to the local electron density of the target material. The methods of Positron Annihilation Lifetime Spectroscopy (PALS) focus on this property by recording the positron annihilation lifetime spectrum to gain detailed knowledge on positron behavior and material properties, information that is valuable for studying and understanding anti-matter phenomena in particle physics. The positron lifetime can be used as a measure for the electron density in solids which allows to draw conclusions on microscopic changes within the atomic lattice of, for example, metal alloys to be used in highly radioactive environments [67].

In a continuous beam, the lifetime is measured with the help of two detectors. One of them sets a start signal which has its origin in the γ-particle that accompanies each β^+-decay of ^{22}Na and is due to the de-excitation into the ground state of ^{22}Ne. The second detector then records one of the annihilation γs and puts the stop signal to the measurement. Other than conventional positron lifetime measurements that use the continuous energy spectrum of a given positron source, slow positron beams use mono-energetic particles. Worldwide, there are a few beams available for positron annihilation studies, offering the possibility to adjust positron energy for depth-sensitive, near-surface material studies. A continuous beam can be used for studying implantation profiles while a pulsed beam additionally measures the positron annihilation lifetime.

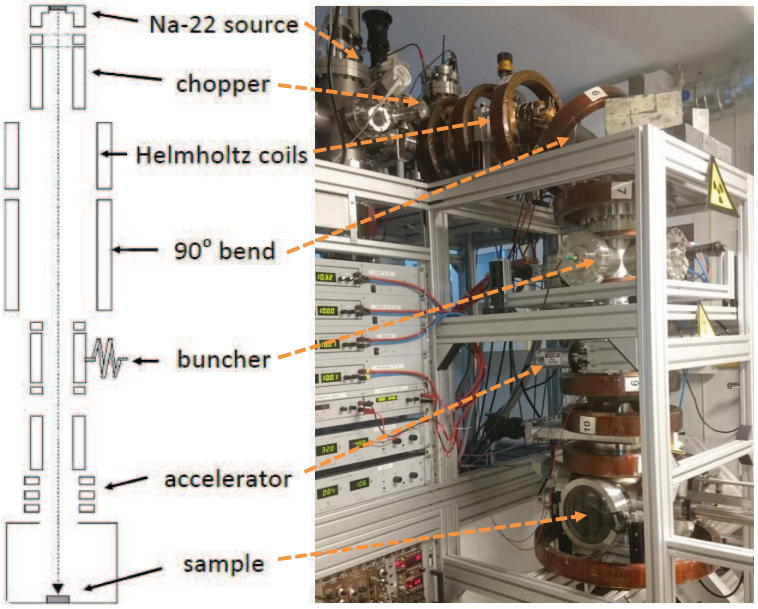

Figure 3.3: The basic configuration of the Chalmers Pulsed Positron Beam.

The Chalmers Pulsed Positron Beam [68] is a vacuum confinement that guides charged particles along a beam line by an arrangement of Helmholtz coils, cf. Fig. 3.3. The Cu-coils create a magnetic confinement for the narrow path of particles. The positrons stem from a source of ^{22}Na where the continuous energy distribution from the β^+-decay peaks at approximately 0.25 MeV and has its maximum at 0.54 MeV [69]. By passing through a thin foil of a well defined moderator material, which in our case is mono-crystalline tungsten (W), the continuous spectrum is transformed into a nearly mono-energetic one. In the moderation process, the energy and amount of positrons is largely reduced due to slowing down and annihilation within the foil but with regard to its thickness of less than 1 micron there are still enough positrons available for material investigations.

A chopper then forms pulses of positrons by applying a sine-shaped potential. These pulses are emitted into the beam line, following the magnetic field lines through a bend, a buncher and a linear accelerator to finally reach the sample chamber containing the material to be investigated. A set of additional, external kick-coils, situated just above the sample holder, is used to straighten the beam line in order to maximize the amount of particles hitting the sample.

The detector is a setup of a BaF_2 high resolution scintillator crystal mounted on a PM tube which is positioned beneath the sample holder. The time distribution of the annihilation γ-rays is recorded by using a data acquisition system with timing measurement. An example of the typical signal shape, as obtained with

the Chalmers Pulsed Positron Beam, is presented in Fig. 3.4 and shows the raw data for positrons annihilating in steel. The data points relate the number of 511 keV γ-rays (y-axis) to their time (x-axis) of creation upon positron annihilation in the sample. The occurring peak in the spectrum is an asymmetric distribution over time with its shape and width mainly determined by beam parameters coupled to the chopper and buncher. The general peak structure changes with respect to positron interactions with the lattice, which leads to differences in the steepness of the left slope. It is here, information on the positron annihilation lifetime components, present in the material, is obtained. The spectrum in Fig. 3.4 also features two peaks of minor intensity further to the left, stemming from the re-emission of positrons into the beam line upon backscattering on the sample surface.

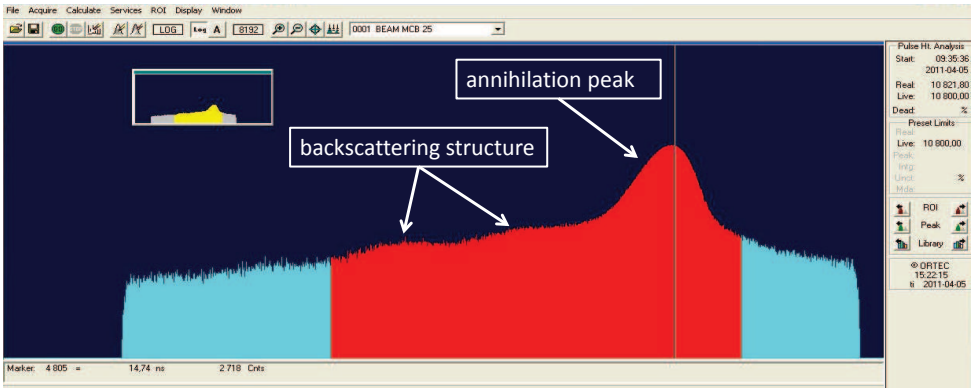

Figure 3.4: Print-Screen of a raw positron annihilation lifetime spectrum as obtained with the acquisition software MAESTRO. The time axis (x-axis) is reversed. Sample: ion-irradiated FeCr alloy; Acceleration energy: 5 keV; Measurement time: 3 hrs.

3.3.3 Lifetime Extraction

The overall shape achieved by the time distribution of the annihilation γ-rays is a convolution of two empirical functions [70, 71]. The empirical resolution function $R(t)$ depends on several beam parameters and is specific for each set of measurements. It is a sum of three or four weighted Gaussian distributions G where each is convoluted with an exponential function to both sides in order to adjust the tails to the left (l) and right (r) of G. Every Gaussian is characterized by its "Full Width Half Maximum" $FWHM$ and the parameters τ_l and τ_r are the shape parameters of the exponentials. Thus, $R(t)$ writes as:

$$R(t) = \sum_{j=1}^{m} f_j G_j(FWHM_j) \otimes \exp\left[-\frac{t}{\tau_{l,j}}\right] \otimes \exp\left[-\frac{t}{\tau_{r,j}}\right] \tag{3.4}$$

In order to analytically describe the recorded annihilation spectrum, a lifetime intensity function $I(t)$ is convoluted with $R(t)$. It describes the positron lifetime components found within a material and is a sum of weighted exponentials:

$$I(t) = \sum_{i=1}^{n} \frac{I_i}{\tau_i} \cdot \exp\left[-\frac{t}{\tau_i}\right] \tag{3.5}$$

$I(t)$ contains specific information on the annihilation lifetime values τ_i which are measures of defect size and their weights I_i which are measures of defect concentration.

All measurements made with the Chalmers Pulsed Positron Beam are of relative nature, meaning that the resolution function $R(t)$, cf. Eq. 3.4, has to be defined prior to any extraction of eventual lifetimes. Thus, a reference sample with well known lifetime intensity function $I(t)$, cf. Eq. 3.5, is necessary in order to perform successful PALS analysis. The positron lifetime does not account for the transport of positrons by the beam and is defined as the time between material entrance and annihilation. A few different algorithms or programs for finding $R(t)$ and $I(t)$ are available [72,73].

All following lifetime extractions are made with the LT program [74] with $R(t)$ being parameterized by 4 exponentially-folded Gaussians. The lifetime intensity function uses either one or two components. The first component describes the bulk-lifetime, the second one is usually used as damaged component and is regardless of defect size. If information on the density of specifically sized defects was to be obtained, the damaged component may be split into more but due to the already large number of variables needed for fitting the data, the uncertainty would quickly increase to a level where conclusions are no longer reliable.

3.4 Depth Profiling

As a sort of calibration study and for gaining a deeper understanding of the Chalmers Pulsed Positron Beam, a project on the penetration depth and restrictions of the beam was initiated.

Furthermore, depth profiling is useful when studying the effects of ion-irradiated samples. As explained earlier in section 2.2, ions serve the purpose of simulating long-time neutron irradiation as it is assumed that subsequent radiation-induced lattice deformations are comparable to each other. However, radiation damage as introduced by ions results in a near-surface damage profile and is complicated to investigate in a non-destructive manner. Consequently, low-energetic positron beams, with a typical range of a couple of nm in a material, present a helpful tool for investigating the nature of radiation-induced material defects which in turn is an important issue when searching for suitable Generation IV and fusion materials. The results of this work on depth profiling are published in paper I.

3.4.1 Au-layered Silica

The positron annihilation lifetime depends strongly on the kind of material and it is this property that was exploited in the experiment used to relate positron acceleration and depth of annihilation. The sample design for the purpose of positron penetration depth studies with the Chalmers Pulsed Positron Beam is based on the large differences in bulk lifetimes for fused silica and gold. Consequently, the decaying slopes of the recorded positron lifetime annihilation spectra of the two materials vary significantly from each other.

The available transparent disk of fused silica was firstly investigated by energy-dispersive X-ray spectroscopy (EDX) and cut to smaller plates (14×14 mm) which were evaporated with Au for thin-film deposition with a Balzers System BAK600 Evaporator. A QCM monitor was used to control the desired Au-layer thicknesses of 10, 25, 50, 80, 130, 200, 300 and 400 nm which, in case of the thinnest layers, were measured for verification with a VeecoDektak D150 Surface Profiler. All samples were manufactured at the "MC2 Nanofabrication Laboratory" at Chalmers University of Technology.

3.4.2 Monte Carlo Simulations

The Monte Carlo code PENELOPE-2008 is used to simulate transport phenomena of electrons, positrons and photons for calculations of particle penetration and energy losses in matter [75]. In the case of electron or positron motion, elastic and inelastic scattering as well as bremsstrahlung or annihilation are treated. For the simulation of positron penetration depth, PENELOPE is used to calculate the point of annihilation, i.e. the distance of positrons moving in the medium

until terminated by annihilation. The included mechanisms of positron trapping are not considered by the code [76].

The input material files needed for running PENELOPE are created in an auxiliary program which extracts physical information and atomic interaction data from the PENELOPE database. The database collects information for a set of 280 materials for elements with Z-number 1 to 99 and a huge amount of common material compounds including SiO_2 (fused silica). Simulations for input geometries as given by the manufactured samples were performed for a number of positron energies, ranging between 1.5 and 13 keV. Each simulation uses 10^6 particles. Fig. 3.5 is an example of the outcome of one such calculation and shows the number of positrons with initial energy 2.5 keV as a function of penetration depth which marks the point of annihilation. The positrons enter the material surface from the right. The shape of the curve changes at the material boundary, indicating that positrons move further in fused silica than in Au, and the fraction of positrons annihilating in Au can be calculated.

At constant positron energy, more particles will be stopped within the Au-layer as it increases in thickness. At constant Au-layer thickness, more particles will traverse the material boundary as their kinetic energy increases. A Au-layer of 400 nm is thick enough to maintain principally all 13 keV positrons within the Au. The fraction of positrons annihilating in Au can then be related to measurements of the positron annihilation lifetime which uses the weight of the lifetime intensity function as an expression for the trapping of positrons in Au.

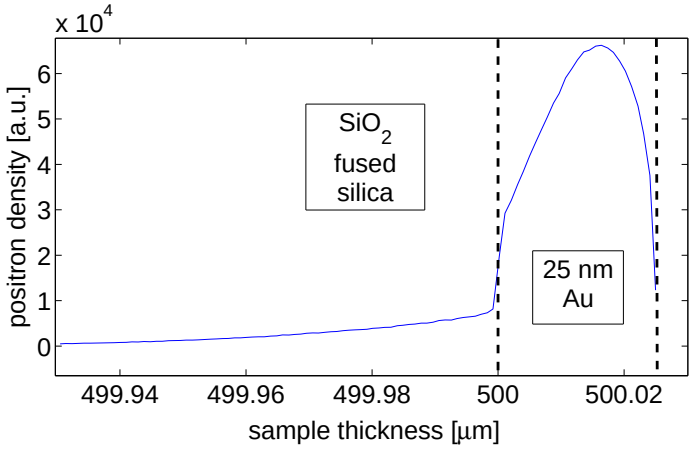

Figure 3.5: PENELOPE simulation for a 25 nm Au-layer on fused silica, displaying number of positrons as a function of sample thickness. The initial positron energy is 2.5 keV. Note that positrons enter the material surface from the right at a thickness of 500.025 μm.

3.4.3 Lifetime Measurements

The Chalmers Pulsed Positron Beam was used to measure the lifetime intensity function of positrons annihilating in Au for the purpose of depth profiling. A total of 4 samples are used for each set of measurements whereas two of them are reference samples. The one required for obtaining the positron resolution function is the fused silica sample with a 400 nm Au-layer. The other one is a sample of pure fused silica, needed for the extraction of the complex lifetime component. The positron energy for each set of measurements is selected in accordance with results from previous PENELOPE simulations, ranging between 1.5 and 13 keV. The samples that were chosen for the measurements have Au-layers of 10, 25, 50, 80 and 130 nm. The measurement time per sample was 4 hours. The raw-data from the measurement run at 3.5 keV positron energy for samples of 25 and 50 nm Au-layer is shown in Fig. 3.6. It can be observed that the overall shape of the lifetime spectra of any Au-containing sample differs significantly from the pure fused silica sample. The huge difference in slope of the main peak holds information on the relative probability for positrons annihilating in either of the materials.

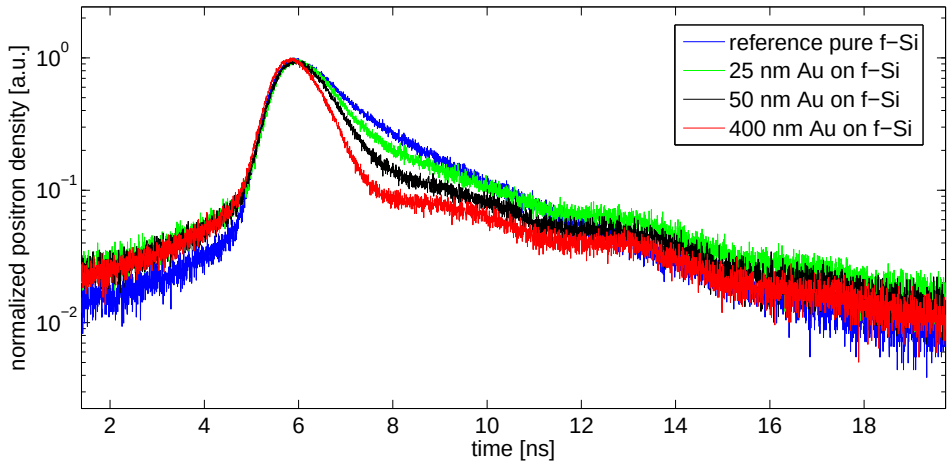

Figure 3.6: Measured positron annihilation lifetime spectra at 3.5 keV for the comparison of raw-data in 0, 25, 50 and 400 nm Au-layer. Note that the time displayed on the x-axis is increasing as opposed to Fig. 3.4.

The LT program is used for the data analysis by de-convoluting the measured spectrum into a positron resolution function $R(t)$ and a lifetime intensity function $I(t)$, cf. subsection 3.3.3. While $R(t)$ is unique for each set of measurements, $I(t)$ is unique for each Au-layered sample and positron energy since it has two lifetime components that change in weight with respect to the amount of positrons annihilating in Au and fused silica. That way, depth profiles such as presented in Fig. 3.7 can be obtained. Here, the fraction of positrons annihilating

in Au is plotted as a function of high voltage for different layer thicknesses and it can be calculated that the penetration depth increases by approximately 20 nm per kV.

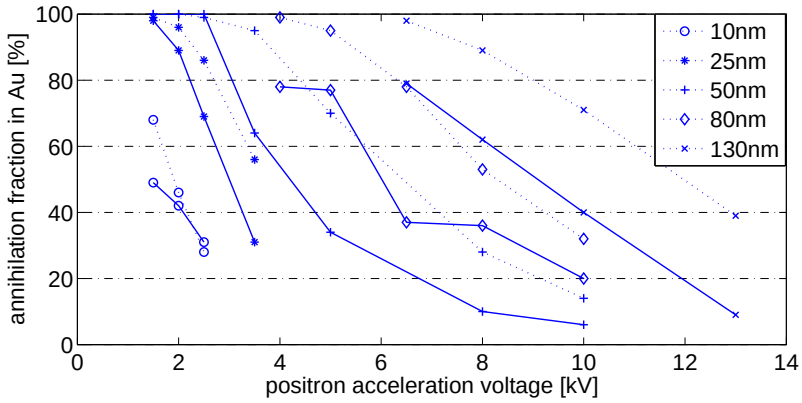

Figure 3.7: Measured (solid) and simulated (dashed) depth profiles for positrons annihilating in Au.

3.4.4 Conclusions

With the help of measurements and Monte Carlo simulations it was possible to obtain depth profiles that are useful for the calibration of the Chalmers Pulsed Positron Beam. The methods agree relatively well with each other even if PENELOPE systematically overestimates the fraction of positrons deposited in Au. The differences between the experimental and simulated results in Fig. 3.7 are, on the one hand, due to theoretical models used by PENELOPE. The code simplifies the real nature of positron interactions with matter by omitting trapping mechanisms in defects and material interfaces. On the other hand, the fitting procedure with the LT program and measurements for characterizing the samples add uncertainty to the obtained results. At positron energies below 6 keV, the penetration depth is smaller than 100 nm which seems to be in contradiction to the theory on positron diffusion with a length scale of approximately 100 nm at room temperature. A possible explanation for this behavior may be motivated by the existence of defects in the lattice of the Au-layer, enabling positron trapping as a stronger mechanism than diffusion.

CHAPTER

4

Steel Alloys

Two long-time projects involving PALS measurements are part of the thesis and deal with the study of neutron-induced radiation damage to materials that present possible candidates for future reactor steels and their use as large internal core-components. The results from the international collaboration GETMAT are summarized in a number of yearly status reports (not included in this thesis) as well as papers II and III. Like GETMAT, the Swedish research program GENIUS, aimed at studying alloys for the possible use in the lead-cooled training reactor ELECTRA. All GENIUS results are summarized in the status reports of the project (not included in this thesis) and the final findings are attached to this thesis in form of section 4.2.

4.1 GETMAT

GETMAT is a European collaborative research project to identify and treat issues concerning structural materials for core components to be employed in future Generation IV and transmutation systems (ADS). Suggested materials have to withstand high temperatures, corrosion and high burn-ups in order to guarantee operational safety during the reactor's lifetime and possible candidates are Ferritic/Martensitic steels with a Cr content of about 10% or ODS steels. In the case of the latter one, there is a lack of experience from nuclear power reactors but certain material properties put ODS steels in focus [77].

Generally, the GETMAT project addresses five priority subjects:

- Improvement and extension of 9-12 Cr F/M steels qualification;
- ODS alloys development and characterisation;
- Joining and welding procedures qualification;
- Development and definition of corrosion protection barriers;
- Improved modelling and experimental validation.

The knowledge gained from decades of nuclear research and reactor operation experience shows that there is a synergy between irradiation and environment that affects material properties. Furthermore, it is certain that phenomena observed during and after irradiation are non-linear and the prediction of material responses may be highly uncertain. This requires a deep understanding of basic mechanisms on the atomic level which is mandatory for the safe operation and design of future nuclear installations [78].

The work performed at Chalmers University of Technology lies within the work package "Microstructure and microchemistry characterisation of ion-irradiated FeCr alloys (concentration, dose and temperature effect): TEM, PAS, APT and Synchrotron techniques" [79] and concentrates on modelling-oriented experiments performed with the Chalmers Pulsed Positron Beam. The measurements were aimed at correlating micro-structural changes upon ion-irradiation and alloy composition. It turned out, that material composition had less effect on the behavior of defects than the irradiation parameters used for the experiment. The GETMAT results are summarized in papers II and III.

4.1.1 FeCr Specimen

The chosen chemical composition of the materials, cf. Table 4.1, is a result of an earlier research project carried out by SCK-CEN (MIRE-Cr Program). Thin plates of the model alloys were fabricated at the University of Ghent, Belgium by furnace melting of industrial purity Fe and Cr that were then annealed for 3 hours at 1320 K in high vacuum. This austenisation and stabilization process was followed by air cooling to room temperature. Full martensitisation was ensured by a 4-hour tempering procedure at about 1000 K.

Table 4.1: Composition of the FeCr alloys.

alloy no.	Mn	P	Al	Ti	**Cr**	Ni	Cu	C	N	O
251	0.009	0.013	0.003	0.004	**2.36**	0.044	0.005	0.008	0.017	0.03
259	0.02	0.011	0.0033	0.0028	**4.62**	0.06	0.01	0.02	0.012	0.06
252	0.03	0.012	0.0069	0.0034	**8.39**	0.07	0.01	0.02	0.015	0.06
253	0.03	0.05	0.003	0.0037	**11.62**	0.09	0.01	0.028	0.023	0.03

After polishing and electro-chemical treatment, all alloys in Table 4.1 but 251, were ion-irradiated at the HZDR (Helmholtz-Zentrum Dresden-Rossendorf) Ion Beam Center. As mentioned earlier, cf. 2.2, irradiation experiments use ions to simulate neutrons for several reasons: high doses can be achieved in comparatively short time, the irradiation range is easily adjusted by ion energy, the availability and flexibility of ion beams is by far larger than offered by neutron facilities and activation is not an issue.

In the case of the chosen GETMAT-alloys, Fe-ions with varying kinetic energy were used in order to obtain a shallow damage plateau [80], cf. Fig. 4.1. Further irradiation parameters are summarized in Tables 4.2 and 4.3.

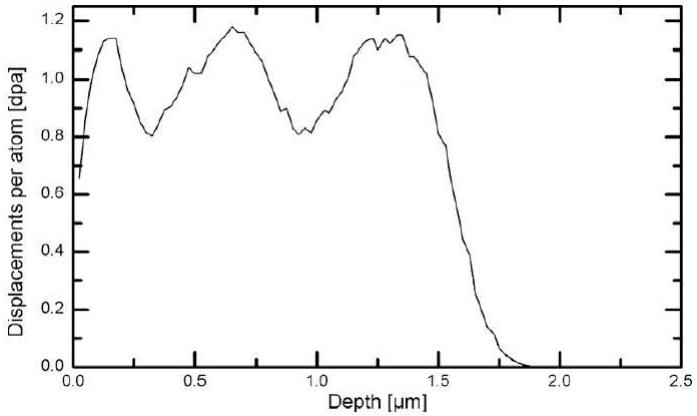

Figure 4.1: Damage profile for three-step Fe-ion irradiation in Fe-9at.%Cr at 1 dpa. [80]

Table 4.2: Irradiation conditions to achieve dose of 1 and 5 dpa, respectively.

energy [keV]	dose for 1 dpa [Fe-ions/cm2]	dose for 5 dpa [Fe-ions/cm2]
500	1.82e14	$5 \times 1.82e14$
2000	2.86e14	$5 \times 2.86e14$
5000	5.62e14	$5 \times 5.62e14$

A number of GETMAT alloys were mounted onto an electrically-heated sample holder which was then placed into the ion beam line. The beam energy was adjusted to different energies thus creating a damage plateau near the material surface. A first set of irradiated samples did not consistently increase or decrease the Fe-ion energy during irradiation which later turned out to be of concern. In a second set of sample irradiation, the three alloys received 5 dpa at the highest temperatures with the ion-energy only increasing. The irradiation conditions for SET 1 and SET 2 are presented in Table 4.3.

Table 4.3: Irradiation pattern for samples 5Cr (259), 9Cr (252) and 12Cr (253).

		100°C	300°C	420°C
SET 1 1 dpa	5Cr	n.a.	$0.5 \rightarrow 2 \rightarrow 5$ MeV	n.a.
	9Cr	$5 \rightarrow 2 \rightarrow 0.5$ MeV	$0.5 \rightarrow 2 \rightarrow 5$ MeV	$5 \rightarrow 2 \rightarrow 0.5$ MeV
	12Cr	n.a.	$0.5 \rightarrow 2 \rightarrow 5$ MeV	n.a.
SET 1 5 dpa	5Cr	n.a.	$5 \rightarrow 2 \rightarrow 0.5$ MeV	n.a.
	9Cr	$0.5 \rightarrow 2 \rightarrow 5$ MeV	$5 \rightarrow 2 \rightarrow 0.5$ MeV	$0.5 \rightarrow 2 \rightarrow 5$ MeV
	12Cr	n.a.	$5 \rightarrow 2 \rightarrow 0.5$ MeV	n.a.
SET 2 5 dpa	5Cr	n.a.	$0.5 \rightarrow 2 \rightarrow 5$ MeV	$0.5 \rightarrow 2 \rightarrow 5$ MeV
	9Cr	n.a.	$0.5 \rightarrow 2 \rightarrow 5$ MeV	$0.5 \rightarrow 2 \rightarrow 5$ MeV
	12Cr	n.a.	$0.5 \rightarrow 2 \rightarrow 5$ MeV	$0.5 \rightarrow 2 \rightarrow 5$ MeV

4.1.2 Measurements

A large number of measurements were performed in the framework of the GETMAT collaboration and lots of knowledge on the performance of the Chalmers Pulsed Positron Beam was gained. The measurements made throughout the years 2009 to 2012 can be divided into four packages:

1. Preliminary test measurements of un-irradiated, as-received specimen did not reveal significant information on the interdependency of lifetime and Cr-content as is expected since the amount of Cr in the atomic lattice of the alloy does not alter the electron density significantly. For the test run, three alloys with 2.36, 8.39 and 11.62 % of Cr were chosen, i.e. 251, 252 and 253, respectively. A thin plate of annealed, pure iron served as reference for the 4-hour lasting measurements. Positron annihilation lifetime spectra were recorded for each sample at 5 and 15 kV positron acceleration which can be approximated to a penetration depth of 100 and 300 nm, cf. paper I, respectively.

2. PAL spectra were recorded for all samples of SET 1 - alloy numbers 259, 252 and 253. The measurement time was 3 hours per sample and acceleration voltages were set to 5, 8, 10 and 13 kV. A measurement series is specified by its beam parameters which are adjusted with respect to positron energy. Each series includes 4 samples whereof 2 are different reference samples. These were an electro-polished, un-irradiated specimen of the respective model alloy and a thin Au sample such as used for the study on depth profiling, cf. section 3.4. In addition to this, the high-temperature, irradiated alloys (1 or 5 dpa at 420°C) served as references for the 9Cr measurement series because they exhibited the most narrow lifetime spectrum in a se-

ries. It was concluded that the high-temperature samples were the most defect-free ones. This is attributed to the lifetime intensity function which is a measure of lattice damage where a steeper slope of the decay part of the peak indicates less material damage.

3. As a consequence of the previous findings, an appropriate reference sample with as little initial lattice damage as possible had to be acquired. Therefore, additional measurements involving several reference candidates were executed as a part of the project. Tested materials were thin foils or plates of mono-crystalline W, Au, Fe and annealed, high-purity samples of Cu and Ni. All candidates were compared to samples of un-irradiated and high-temperature, ion-irradiated 9Cr alloy (252), showing that Cu, Ni and Au coincided very well with the specimen irradiated to 5 dpa at 420°C. However, in the case of Au, it seems as if a back-scattering structure appears at the end of the decaying slope which can be related to the high density of Au and Cu is the preferred reference sample.

4. Finally, PAL spectra were recorded for all samples of SET 2, using Cu as reference material. The measurement time was 3 hours per sample and acceleration voltages were set to 8, 10 and 13 kV. For each alloy, there are 3 measurement series (one per positron energy) and each series uses two references (Cu and Ni) and the two irradiated specimen at 300 and 420°C.

4.1.3 Defect Analysis

The analysis of the measured lifetime spectra is based on the extraction of positron annihilation lifetimes as a function of lifetime and respective weight. While the lifetime value may be used for describing the size of a vacancy-type defect, its weight is a measure of defect density.

A sum of 4 exponential-sided Gaussian functions is used for defining the empirical positron resolution function. The lifetime intensity function for the reference sample consists of one component (100 % intensity) with its lifetime value fixed to 110 $\pm$ 3 ps. All fitted reference spectra differ from the measurements by less than 5%. By unfolding the measured spectra of one series with the fixed positron resolution function, it is possible to gain information on the unknown lifetime intensity function. Taking into account that the measurement and fitting procedure experience lots of uncertainty, it was decided to fix the number of lifetime components to 2 - one for the un-damaged bulk lattice and one for the sum of defects. This simplification is done in order to reduce the number of variables and increase the reliability of the fit. The quality of the fit as achieved by LT is given by the sum of squared residuals which in most cases is very close to 1 and the results of the positron annihilation lifetime measurements are presented in papers II and III.

Paper II summarizes and presents the findings of the GETMAT project in a number of tables and figures. The aim of the study was to relate irradiation conditions such as dose and temperature to the size of defects developed upon irradiation with respect to the Cr-content of the model alloys. The positron annihilation lifetime of a vacancy-type defect is closely related to the size of the defect and hence, the analysis of the measurements in the GETMAT framework attempts to translate the lifetime value of the 2nd component into void size [81]. This way, Fig. 4.2 can be created and it is found that:

- The void size is smallest for the highest amount of Cr, i.e. 12Cr. The amount of voids, i.e. weight of the second lifetime component, is not affected by the Cr-content.
- The void size increases significantly with higher dose. The amount of voids decreases simultaneously, implying that voids cluster together upon increasing dose.
- In case of the low-dose irradiation, the void size is unaffected by the temperature but the amount of voids decreases with increasing temperature. In case of the high-dose irradiation, the void size increases significantly with temperature while the amount of voids is strongly decreasing. Independent of dose, no voids can be observed for the highest temperatures. This analysis is only applicable for Fe9Cr.

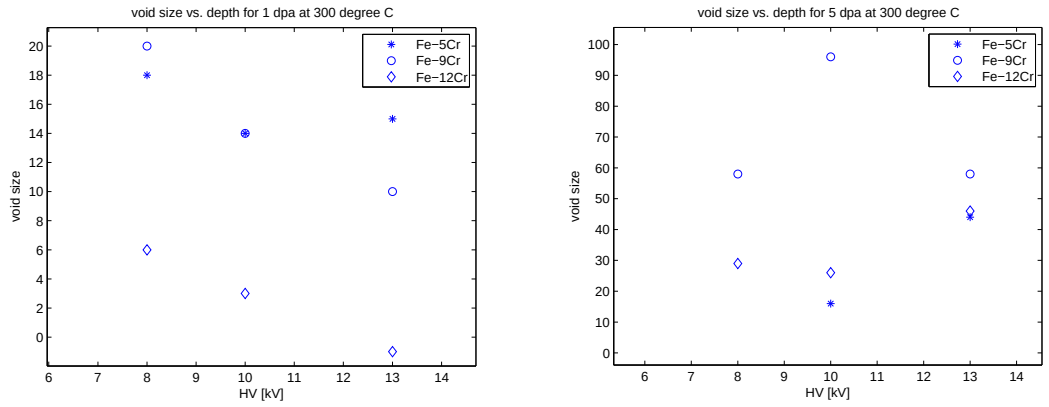

Figure 4.2: Void size given as the number of vacancies in the void as a function of high voltage, i.e. depth, for 5Cr, 9Cr and 12 Cr for doses 1 and 5 dpa at 300°C.

4.1.4 The Importance of Irradiation Parameters

The results from the irradiated GETMAT alloys were further investigated with respect to specific irradiation parameters such as order of ion energy, temperature and dose. Here, a closer look at the weight of the second lifetime component was taken and Tables II, III and IV in paper III show how the concentration of defects is affected by the irradiation procedure. One of the most surprising results of that analysis is re-printed in Tab. 4.4 and presents the change in lifetime weight when the ion-energy used for achieving the intended damage-profile is changed, cf. Tab. 4.3. According to the beam calibration presented earlier, the positrons only reach the near-surface region of the studied alloys (below 300 nm) which is comparable to the range of 0.5 MeV Fe-ions, cf. Fig. 4.1. It is thus seen, that the order of ion energy plays an important role for the defect behavior:

When the ion energy is increased from 0.5 to 2 to 5 MeV, the range of ion implantation increases and irradiation damage is created further inside the material. Towards the end of the irradiation procedure, lattice defects will primarily be produced deep within the material while defects closer to the surface have a high ability to change in character by defect migration, recombination and clustering due to the high temperature of the irradiation procedure [28]. These processes tend to reduce the defect density, thus altering the lifetime intensity function by a decrease in weight.

If instead the ion energy is decreased from 5 to 2 to 0.5 MeV, defects near the surface will be created at the end of irradiation. They have less time to cluster or migrate and the simultaneous production of defects leads to a higher defect density than observed previously.

Table 4.4: Weights of the second lifetime component [%] for investigating the effect of order of ion energy for all alloys irradiated at 300°C to a dose of 5 dpa.

alloy	weight [%] of the second lifetime component					
	order of ion energy: high to low $5 \rightarrow 2 \rightarrow 0.5$			order of ion energy: low to high $0.5 \rightarrow 2 \rightarrow 5$		
	8 kV	10 kV	13 kV	8 kV	10 kV	13 kV
Fe5Cr	61	63	n.a.	6	16	9
Fe9Cr	19	24	63	3	7	9
Fe12Cr	53	n.a.	n.a.	12	13	15

Paper III also sheds a light on how to treat the dose dependency found in paper II. For achieving a total dose of 5 dpa, the alloys were irradiated at the same rate as the 1 dpa case but 5 times as long. Therefore, the high dose samples were heated over a longer period of time and it is difficult to state which of the two

parameters mainly contributes to the observed effects. While the weight of the second component is decreasing with higher dose and/or longer heating, the lifetime is increasing even if ns-lifetime values with usual weights below 7% are highly uncertain due to a very low peak-to-total ratio.

Finally, it is concluded that migration and recombination of defects alter the micro-structural behavior of materials in an unpredicted manner so that studies used to simulate neutron-damage by ion-irradiation experiments have to be planned and executed under great control.

4.2 GENIUS

The GENIUS project (active between 2009 and 2012) was a national collaboration between the Swedish universities KTH, Uppsala University and Chalmers, financed by the Swedish Research Council (Vetenskapsrådet) [82]. The focus of the project was on research and development of technology for Lead-Cooled Fast Reactors (LFR). Parts of the knowledge gained from the three work packages on fuel development, materials research and safety evolved into the attempt of designing and building ELECTRA (European Lead Cooled Training Reactor) which aims at LFR dynamics research, education and training [83, 84]. One of the Chalmers contributions to the work package on materials research (WP2) consists of measurements of radiation induced defects in irradiated alloy samples [85].

4.2.1 FeCrAl Specimen

A number of FeCrAl alloys were manufactured in cooperation with Sandvik Heating Technology AB (Sweden) for investigations of corrosion properties performed by the Department of Surface and Corrosion Science (KTH) and Materials Microstructure (Chalmers) [86]. Three alloys were used for positron annihilation lifetime measurements with the Chalmers Pulsed Positron Beam in order to study micro-structural changes of the alloys upon ion irradiation. The bulk alloy compositions are given in Tab. 4.5.

Previous experience from the GETMAT collaboration showed that ion irradiation conditions need to be well controlled and the irradiation procedure was planned in accordance to the knowledge gained at that time. The irradiation experiment was executed at the IonTechnologyCentre at Uppsala University and uses Fe-ions with an implantation energy of 250 keV, corresponding to a deposition depth of approximately 200 nm (SRIM). In order to achieve a shallow damage region, the ion energy was chosen so that defect production occurs closer to the surface than the maximum positron penetration depth of more than 300 nm. The irradiation temperature was kept constant at 25°C and doses of 1, 0.1 and 0.01 dpa were achieved by adjusting the irradiation time.

Table 4.5: Bulk composition of the FeCrAl alloys [87].

alloy	Fe	Cr	Al	Si	C	Ti	Zr
10Cr-8Al	81.75	10	8	0.07	0.03	0.07	0.08
10Cr-6Al	83.75	10	6	0.07	0.03	0.07	0.08
10Cr-4Al	85.75	10	4	0.07	0.03	0.07	0.08

4.2.2 Results and Conclusions

Positron annihilation lifetime spectra were recorded at positron energies 10 and 15 keV with the measurement time set to 3 hours. Lifetime component analysis with the LT program was not performed due to insignificant differences between the measured spectra and conclusions are merely based on observations made on the recorded raw data.

At first, measurements of the as-received state of the un-irradiated alloy-samples were compared to a reference of seemingly defect-free HPCu. In Fig. 4.3, it can be seen that the Cu-reference exhibits the steepest slope, but even the shapes of the remaining spectra are strikingly similar. It is concluded that the 6Al and 8Al references are as defect-free as the Cu-reference and that only the 4Al sample seems to contain non-negligible amounts of lattice defects as a result of the manufacturing process.

Then, samples that received doses of 0.01 and 1 dpa as well as two references were used for investigations of the influence of dose upon Fe-ion irradiation. Each set of measurements uses the same alloy composition and the references are the un-irradiated specimen of the alloy and the HPCu sample. Excerpts of the raw data obtained for all alloy compositions are shown in Fig. 4.4.

4.2.3 Conclusions

From investigations of the obtained raw data, it was observed that the main peak of the lifetime spectrum widened, even if not significantly, with increasing dose. This implies that positron trapping is intensified or that the positron annihilation lifetime is increased at higher doses and is attributed to the increased size or amount of vacancy-type defects created upon ion-irradiation. In contrast to the GETMAT irradiation, a dose dependence is concluded since temperature effects on defect kinetics can be neglected. It is also stated that micro-structural changes due to radiation exposure do not seem to depend strongly on the bulk composition of the investigated alloys.

It is surprising that the differences between the samples are small considering the relatively high irradiation dose of 1 dpa. We may have errors that are related to sample preparation, irradiation procedure or false initial assumptions which are likely to influence sensitive PAL measurements in such a way that reliable lifetime component extraction is not applicable as was the case in this study.

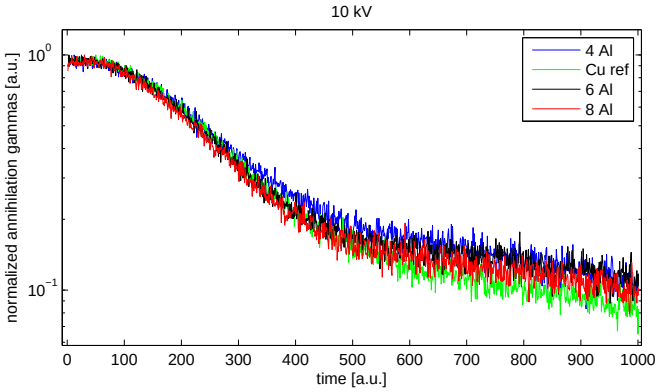

Figure 4.3: Excerpt from PAL spectra for un-irradiated alloys and HPCu reference sample at 10 keV positron energy. The time on the x-axis is given in arbitrary units.

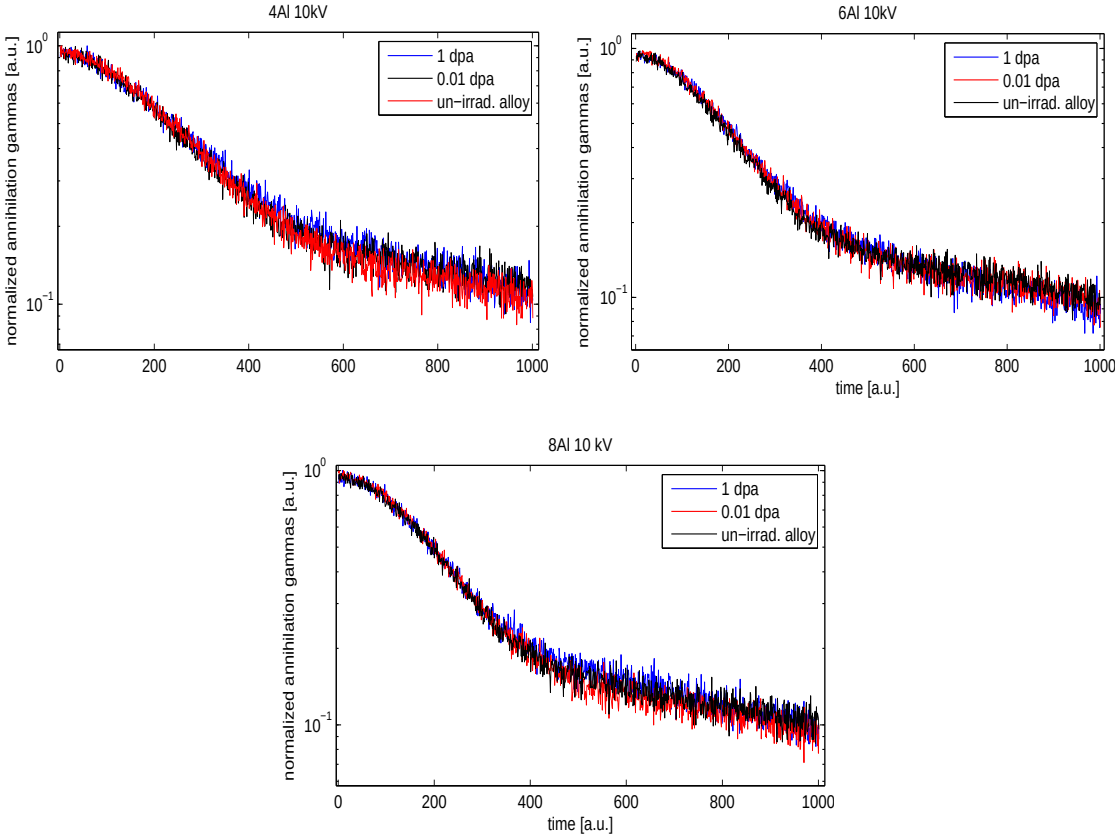

Figure 4.4: Excerpts from PAL spectra for irradiated alloys and un-irradiated alloy reference at 10 keV positron energy. The time on the x-axis is given in arbitrary units.

Part II

Nuclear Safeguards and Emergency Preparedness

CHAPTER

5

Introduction

5.1 On the Safety of Radioactive Materials and the NPT

The concept of "Nuclear Safeguards" was developed around mid-1900 out of the need for tools that shall help to control the global spread of nuclear materials for various purposes and aims primarily at the prevention of nuclear war and related military actions. Within safeguards, a number of legal measures and scientific techniques are applied to verify the completeness and correctness of information provided by all countries with access to any kind of nuclear materials. As a direct consequence of this, the IAEA (International Atomic Energy Agency) was formed in 1957 [88, 89] as an autonomous organization with the mission to promote the peaceful use of nuclear energy and its safety.

A decade later, in 1968, the Treaty on the Non-Proliferation of Nuclear Weapons (NPT) was initiated [90,91]. The NPT is a form of contract that prohibits any form of military exploitation of nuclear materials and furthermore encourages the decommissioning of existing warheads. Today, all nuclear weapon states as well as almost all other nations support the general terms of the treaty and thus agree on the solely peaceful use of nuclear power.

Radionuclides that are primarily surveilled with the help of national and international nuclear safeguards measures can be categorized as [92]:

- nuclear fuel and spent fuel;
- radioactive waste from various nuclear industries;
- weapons-grade nuclear materials;
- medical isotopes and industrial sources.

Figure 5.1: Stamp to celebrate Dwight D. Eisenhower's "Atoms for Peace" speech at the UN General Assembly in New York, 1953. His ideology led to the creation of the IAEA [93].

There are different methods that make nuclear safeguards work in reality. These are in principal divided into three constantly-developing branches:

- A number of bureaucratic procedures are initiated on the basis of legislation, administration and documentation. National and international authorities then have to make sure, that all obligations are followed by the actors that deal with any kind of nuclear materials.
- The surveillance of known radiation sources happens to a large extent by measurements. The results are part of the bureaucratic branch and are partly used for validating the documentation of radioactive sources that are used for various purposes such as industry, power production, research or medical care.
- While in the previous, measurement techniques are used to validate the inventory of sources, the forensic branch applies measurements for locating nuclear materials that may lack documentation. Such unknown sources present a hazard if handled incorrectly so that this branch of safeguards craves special attention and partly other approaches than conventional verification methods.

Even the computational approach is tightly bound to experimental methods and is often necessary for validation and benchmarking purposes. The safeguards-related work that follows, focuses on experiments within the latter two branches and how liquid scintillation detectors can be used to identify radiation sources by type and/or strength.

5.2 Emergency Preparedness - what if...?

The Swedish Civil Contingencies Agency MSB (Myndigheten för samhällsskydd och beredskap) aims at protecting certain values of the Swedish society such as human rights, health and freedom, democracy and justice, environment, economics and national sovereignty. It does so by being responsible for coordinating operations and providing resources that help to protect individuals as well as society and prevent further consequences in the happening of national or international disasters and natural catastrophes. Here, action plans and guidelines for how to act quickly and how to distribute necessary tasks efficiently are tools for being prepared if the emergency becomes a fact. The list of involved actors stretches from public institutions over private businesses down to voluntary organizations, all with varying levels of influence depending on the magnitude of the situation (local, regional, national, EU, international) [94].

A number of scenarios have been classified as being a threat to the values of the Swedish society. These can be aspect to national and individual security, infrastructure or weather conditions as well as industrial accidents related to chemical, medical or nuclear emergencies. With respect to the potential threat originating from any kind of nuclear materials, the MSB identifies nuclear power emergencies as the only case in need of emergency preparedness routines. However, radioisotopes are widely used within other applications not related to nuclear reactors. Such sources may, if handled incautiously and incorrectly, present a significant risk to people's health and the environment.

The objective of nuclear safeguards is to gain knowledge and control over various radioactive sources through legal frameworks and surveillance methods but even the most thorough routines can be subject to failure. While nuclear materials related to the power industry are rigorously controlled, less awareness of the threat coming from radioisotopes in general may be present in a large number of other areas and radiological accidents either involving specific isotopes or nuclear materials can happen on many levels. While a power reactor accident is the most obvious scenario, its likelihood is very small. Frequent transportation of nuclear fuel (fresh, re-processed or used) at land and sea presents a risk of environmental contamination. Laboratory and medical sources are often strong and may be object to theft, the miscalibration of radiotherapeutical instruments can lead to unintentional radiation exposure. Industrial as well as ”forgotten” sources or scrap metal may lack sufficient surveillance, radiation shielding or storage and foremost knowledge.

In any case, the aim of all taken actions after an accident scenario is to minimize the possibilities for individual and environmental contamination and reduce radiation effects to living organisms due to the uptake of radioisotopes.

CHAPTER

6

Radiation Detection

The fields of nuclear safeguards and emergency preparedness that are being introduced in chapter 5 are closely related to each other by the methods used for experimental and theoretical research. Both areas cope extensively with the detection of directly and indirectly ionizing radiation so that a quick overview of radiation detection techniques, partly used within the studies presented in papers IV through VIII, is given here.

To repeat, radiation is the emission of energy in the form of electromagnetic waves or subatomic particles. To measure the amount of ionizing radiation from a radioactive source and thus estimate its effects on matter, physical interaction properties are made use of in the field of radiation detection.

The very early beginnings of radiation detection are found within the evolution of photography and the invention of the dry photographic plate in 1879. In 1896, H. Becquerel found that naturally fluorescent minerals would develop dark spots on a dry plate, indicating the presence of invisible light, namely highly-penetrating gamma-radiation. Many experiments later, he showed that different substances emit even other types of ionizing radiation since these could be bent by magnetic fields. The discovery of α, β and γ radiation marks the beginning of radiation detection techniques. It leads to the development of the field of nuclear physics which describes the interaction mechanisms of nuclei, and presents a milestone within atomic and particle physics [95].

Different types of ionizing and non-ionizing radiation, such as α, β, γ and neutrons, interact with matter in different ways and thus, detection techniques vary in accordance to measurement purposes due to different physical properties of the energy transfer [96]. Detectors come in almost countless kinds and sizes, all having one thing in common: a sensitive volume produces a signal which is

directly related to the interaction of incident radiation with the electrons or nuclei of the active volume. For a wide category of detectors, such a signal induces a small current which then is representative for the interaction mechanism of the particular radiation.

6.1 Gas-filled Detectors

Radiation detectors known as ion chambers, proportional counters and Geiger-Müller counters (commonly referred to as Geiger or GM-tubes) belong to the oldest and most widely used devices for the detection of directly and in-directly ionizing radiation. All of these are based on the ionization and excitation of gas molecules due to the passage of charged particles, either directly originating from a source or as a result of interactions with the incident particle. The ions that are created within the gas-filled volume of a detector will drift according to their charge as an electrical field is applied. The subsequent ionization current that is accumulated at the electrodes is proportional to the number of ion-pairs created in the gas and can be measured by an electrometer [97].

Ion chambers can be operated at comparatively low voltages and are efficiently used to detect radiation from particles of energies 10 keV and higher. Since the number of ion-pairs is an indirect measure of the absorbed dose (amount of deposited energy per unit mass), ion chambers are frequently used as radiation survey instruments that allow to locate sources and quantify the dose to its surroundings. Particle discrimination is not featured when using ion chambers.

Geiger tubes and proportional counters are types of gas-filled detectors that are operated at higher voltages than ion chambers. This leads to gas multiplication during the drift of the ion-pair initially produced in a particle-gas-interaction so that even single ionization events from low-energetic particles can be detected. While in a GM-tube all particles create the maximum number of avalanches, proportional counters may be used for particle and energy discriminating measurements. With increasing particle energy, the number of ion-pairs is increasing and calibrations of the collected charge in proportional counters are used for spectroscopy measurements where energy resolution is not the primary focus.

All of the above are frequently used for the measurement of α, β and γ radiation but environments where neutron sources are present remain un-observed due to the interaction properties of neutrons. However, the choice of filling-gas determines the capabilities of the used detector. In the widely used BF_3 proportional tube, boron trifluoride gas is used for converting non-ionizing neutrons into a measurable current of ionizing particles. This is possible since ^{10}B has a high absorption cross-section for thermal neutrons, leading to the nuclear reaction:

$$^{10}B(n,\alpha)^{7}Li \tag{6.1}$$

Each nuclear reaction then produces an ion-pair which will drift to the electrodes of the detector, inducing a charge proportional to the amount of interactions. Furthermore, ionization chambers with an inner coating of fissile material, known as fission counters, can be used for the detection of slow and fast neutrons. This form of instrumentation is typically used for neutron measurements in reactor environments.

6.2 Scintillator Detectors

The conversion of scintillation light into an electrical pulse is useful for the detection and spectroscopy of various kinds of radiation. The choice of scintillation material is governed by a number of criteria such as [97]:

- high efficiency for conversion of kinetic energy into light;
- linearity between conversion yield and deposited energy for a wide energy range;
- transparent to emitted wavelength upon interaction;
- short decay time of induced luminescence;
- good optical quality and workability for large scale applications;
- refractive index of the same order as for the light sensor needed for signal processing.

Active materials for the use in scintillator detectors are categorized as organic or inorganic scintillation materials. Examples of organic scintillators are pure crystals, liquid solution or plastic materials which all emit fluorescent/phosphorescent light upon transitions in the energy level structure of the molecule due to radiative energy deposition. One advantageous feature of organic scintillators is the occurrence of prompt and delayed fluorescence which can be represented by a sum of two exponential decays. The difference in decay time of the fast and the slow component can be used for the purpose of Pulse Shape Discrimination (PSD) since the slow component contains information on the nature of the exciting particle [97]. Thus, the technique of PSD may be applied for the differentiation of γ-induced events in measurements of neutron radiation as is done in the studies presented in this thesis.

A large number of inorganic scintillator materials is available. Their scintillation mechanism is determined by the energy bands of the crystal lattice. Incident radiation may excite an electron from the valence band to the conduction or exciton band. This results in a loose-bound electron-hole pair which eventually is captured by lattice impurities where the electron can de-excite to the valence band, giving rise to the emission of a scintillation photon. In order to measure

positron annihilation lifetimes with the Chalmers Pulsed Positron Beam, a high time resolution to the 511-keV annihilation spectrum is required. This is achieved by using a small crystal of BaF_2 which has a fast decay time component of 0.6 ns. A much more frequently used material for large scintillator detectors is NaI which is made use of in a number of applications for dosimetry measurements such as whole body counters.

For the collection of the light produced in any scintillator, the sensitive volume is mounted onto a photo-multiplier/photodiode which is needed for light conversion and signal amplification into a measurable electrical pulse.

6.3 Semiconductor Diode Detectors

In cases of radiation measurements that require a high energy resolution, semiconductor diode detectors are often the preferred choice. The most frequently used semiconductor materials are silicon and germanium crystals. For energy-sensitive γ-ray measurements, high-purity Ge (HPGe) detectors are widely applied [97]. Just like in inorganic scintillators, electron-hole pairs are created on the encountering of radiation on the semi-conductor material. Since an electrical field is directly applied to the semi-conductor, the electrons and holes drift to the electrodes, inducing a charge in a way similar to the mechanisms in gas-filled detectors. The energy needed for creating such a pair may be as small as 3 eV and by measuring their amount, the energy of the incident particle can be determined. The probability for valence electrons to cross the band-gap increases with temperature and HPGe detectors are typically cooled with liquid N in order to reduce thermal noise.

A classical feature of energy spectra recorded with HPGe detectors is the occurrence of a Compton plateau due to inelastic scattering of photons on charged particles. Despite that, high-intense Gaussian peaks within the plateau resolve very sharply. When used in neutron environments, peaks may be broadened due to Doppler effects from the motion of neutron-activated atoms that de-excite through γ-emission. It is important to notice that semi-conductor detectors are sensitive to radiation damage so that strong sources may cause irreparable performance degradations. However, HPGe detectors may be restored by annealing the detector material in a high temperature environment

CHAPTER

7

Nuclear Safeguards Measurements

Experimental work comprising neutron and γ-ray measurements has been performed under supervision from the Nuclear Safeguards and Security Group at Nuclear Engineering (Chalmers) and the Division of CBRN[2] Defence and Security at FOI (Swedish Defence Research Agency). The results achieved from the involvement in actions of these research groups are presented through papers IV and V which cover research topics such as nuclear fuel and nuclear forensics, respectively.

7.1 Spent Fuel

For the evaluation of nuclear fuel in a spent fuel pool, a number of non-destructive techniques such as the Cherenkov Viewing Device or the Under Water Neutron Coincidence
Counter can be directly applied at the storage site for irradiated or un-irradiated fuel. The use of boric acid as a thermal neutron absorber, for the purpose of radiation shielding, necessitates corrections to traditional measurements for fuel pool investigations due to the effect of boron on processes like multiplication and detector efficiency [98].

7.1.1 Novel experiments for estimating the amount of B in water

In paper IV, a method is proposed for the independent evaluation of the boron content in a PWR spent fuel pool by using liquid scintillation detectors. The

[2] **C**hemical, **B**iological, **R**adioactive, **N**uclear

idea of the concept is to utilize the γ-energies released upon neutron capture in hydrogen and boron by relating the difference in intensity to the concentration of boron.

The experiment uses a shielded neutron source of ^{252}Cf (decay modes: spontaneous fission 3.09%, α 96.91%) with a neutron yield of about $9 \cdot 10^6$ n/s. It is contained in a block of polyethylene (PE) which can be opened for measurement purposes of the fast neutrons emitted from the source. An EJ-309 liquid scintillation detector is used for measuring the photons released in the nuclear reactions:

$$^1H(n,\gamma)^2H^* \quad E_H = 2223.3keV$$

$$^{10}B(n,\alpha)^7Li^* \quad E_B = 477.6keV$$

The detector is placed approximately 25 cm above the open PE source containment on top of an Al-tank which is filled with 4.2 l of borated water with concentrations varying between 0 and 4200 ppm. The measured signal is recorded in list mode and includes information on timing and energy, making Pulse Shape Discrimination (PSD) for neutrons and γ applicable. For the further analysis, only data points with a PSD index between 0.04 and 0.07 are used in order to eliminate the neutron contribution to the signal, cf. Fig. 7.1. After extracting the γ-counts with respect to their PSD index, the energy spectrum for any of the boron concentrations can be obtained. If no boric acid is added to the water tank the spectrum only shows a contribution from the absorption in H in the high-energy region.

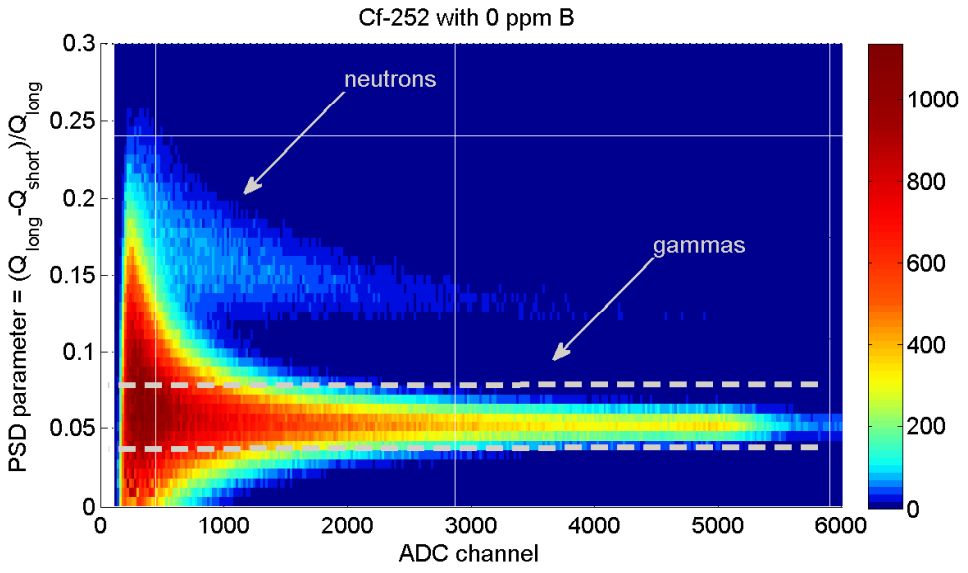

Figure 7.1: Histogram plot for the number of counts as a function of PSD index and ADC channel for ^{252}Cf measurement on non-borated water. Includes indication of PSD range from 0.04 to 0.07.

When boric acid is added to the water, the contribution of the γ-line from the thermal absorption in B is visible in the Compton-plateau of the energy spectrum. An example of measured data for a concentration of 3500 ppm B is presented in Fig. 7.2. Apart from the obtained spectrum for the cases of pure and borated water, Fig. 7.2 also shows the Compton-scattering spectrum of the 477 keV line which is obtained by subtracting the normalized pure-water case from the borated-water case.

The analysis procedure was repeated for B-concentrations of 1500, 2000, 2500 and 3000 ppm and experiments as well as simulations successfully showed, that the intensity of the 477 keV peak is proportional to the amount of dissolved B even if the differences do not seem to be significant under usage of ^{252}Cf as neutron source.

The method performed significantly better when applied to similar measurements with an AmBe neutron source instead, demonstrating that the evaluation of the B-concentration in water is very sensitive to the choice of PSD index [98].

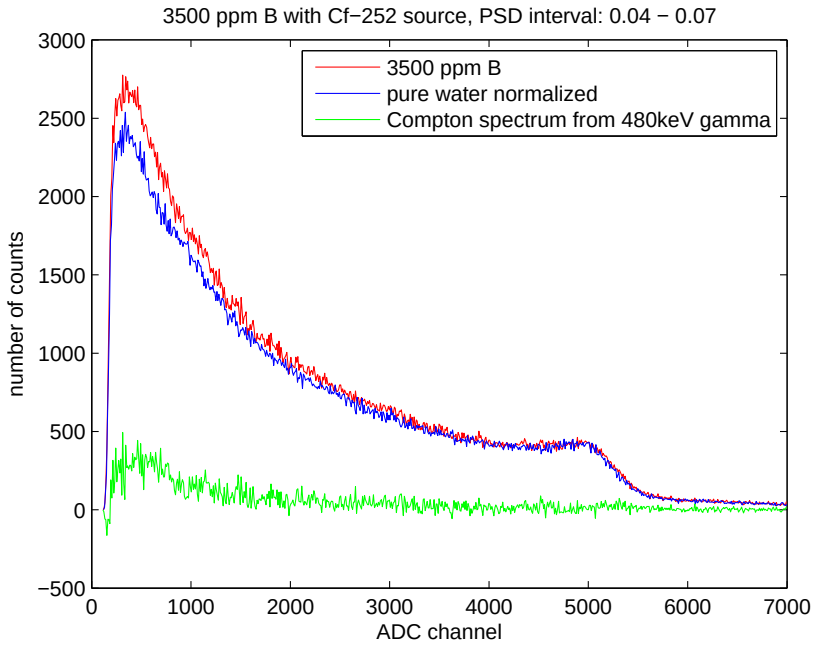

Figure 7.2: PSD-selected counts plotted as a function of ADC channel for 3500 ppm B. The red curve represents the measured raw data, blue is normalized pure water and green is subtraction of both.

7.2 Nuclear Forensics

The field of nuclear forensics concentrates on the development and use of techniques against illicit trafficking of nuclear materials and other criminal activities

related to radioactive materials. As part of the mission of the IAEA, the objectives of the *Code of Conduct on the Safety and Security of Radioactive Sources* [99] lay the foundation for the tasks of national authorities that are involved with nuclear safety and security. The "Code of Conduct" explicitly states that "every state should establish a national register of radioactive sources" which allows to identify and trace sources for the purposes of nuclear safeguards.

A convenient way for the identification of nuclear sources is to use source specific signatures which, apart from serial number, ownership documentation and visual inspection, can be obtained from physical properties inherent in the source by age determination, isotope ratio and impurity measurements. Apart from fissile materials, fissionable radionuclides such as ^{241}Am are subject of forensic investigations as described in paper V. It aims at investigating the possibilities of using γ spectrometry for finding inherent signatures, i.e. age and impurities, of strong ^{241}Am sources.

7.2.1 Characterization of strong Am-241 sources

Strong α-emitting sources may undergo nuclear reactions with preferably light elements, often leading to the emission of neutrons and protons. Elements like F, Na, Al or Mg may be part of the source encapsulation or occur as impurities within the source. Additionaly, the product nucleus is usually in an excited state and will de-excite or decay by the emission of characteristic γ-rays.

For the study presented in paper V, five different ^{241}Am sources were investigated. Part of the characterization of the two strongest sources with a nominal activity of 185 GBq, was to understand initial γ-measurements where the instrument used for the identification of an unknown source interpreted the presence of neutrons and ^{241}Am as Pu.

At first, γ-spectra were recorded for all sources with a HPGe detector. The strongest ^{241}Am sources showed a number of lines not attributed to the radionuclide with some of them being Doppler-broadened (1129, 1779 and 1809 keV) [100]. Additional measurements with liquid scintillation detectors revealed a considerable neutron flux which was too high to originate from the spontaneous fission branch of ^{241}Am ($3.6{\cdot}10^{-10}$ %) and is thus a result of nuclear reactions between the α-particles from the source and low-Z elements. These observations confirm the presence of impurities which may be used as signatures for the strong ^{241}Am sources.

While the γ-spectrum for pure ^{241}Am records transition energies up to approximately 1000 keV and has high-intensity lines in the low-energetic region (up to 100 keV) only, the measured spectrum of the strong sources used in this study stretches up to about 3000 keV. The measured spectrum for source no. 1 (cf. paper V) is presented in Fig. 7.3 where all of the marked peaks can be related to nuclear reactions with the stable isotope ^{23}Na. A selection of probable transitions and respective energies, furthermore indicating the origin of the measured

neutron flux, is presented in Tab. 7.1.

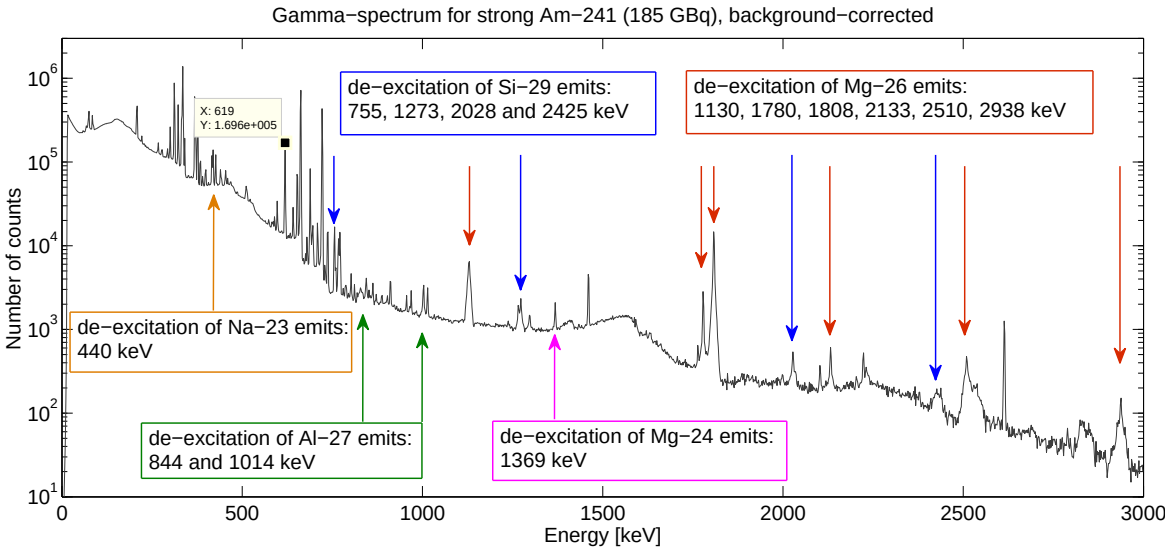

Figure 7.3: Background-corrected γ-spectrum for strong source of ^{241}Am from measurement with HPGe detector with indication of origin of certain characteristic lines.

Table 7.1: Selected nuclear reactions between Am and impurities.

nuclear reaction			decay mode	measured transition energies [keV]					
^{23}Na + α	$\rightarrow$	α' + ^{23}Na*	stable			440			
	$\rightarrow$	γ + ^{27}Al*	stable		844			1014	
	$\rightarrow$	p + ^{26}Mg*	stable	1130	1780	1809	2133	2510	2938
	$\rightarrow$	n + ^{26}Al	^{26}Al $\rightarrow \beta^+$ + ^{26}Mg	1130		1809			2938
^{26}Mg + α	$\rightarrow$	n + ^{29}Si*	stable	755	1273	2028	2425		
	$\rightarrow$	p + ^{29}Al	^{29}Al $\rightarrow \beta^-$ + ^{29}Si	755	1273	2028			
^{23}Na + p	$\rightarrow$	p' + ^{23}Na*	stable			440			
^{26}Mg + p	$\rightarrow$	γ + ^{27}Al*	stable		844			1014	
^{23}Na + n	$\rightarrow$	γ + ^{24}Na	^{24}Na $\rightarrow \beta^-$ + ^{24}Mg			1369			
^{26}Mg + n	$\rightarrow$	γ + ^{27}Mg	^{27}Mg $\rightarrow \beta^-$ + ^{27}Al		844			1014	

The presence of the characteristic line at 440 keV from the de-excitation of ^{23}Na leads to the conclusion that it is contained within the sample in form of impurities, either as part of the matrix or the encapsulation of the ^{241}Am source. By calculating the ratio between the peak areas of well-distinguishable γ-lines from each isotope - in this case 440 keV for ^{23}Na and 619 keV for ^{241}Am - the relative concentration of the impurity element can be estimated and thus be used as a signature for the source. If listed in national and international source libraries, information on inherent source impurities could be useful for investigations related to orphan sources and nuclear forensics.

CHAPTER

8

Simulating Source Distributions in Humans

In cooperation with the the Division of Radiation Physics at Gothenburg University, a study for calibrating the Whole Body Counter (WBC) available through the Sahlgrenska Institute was motivated and financially supported by the Swedish Radiation Safety Authority SSM (Strålsäkerhetsmyndigheten) and MSB.

In case of a radiological accident or emergency situation, correctly calibrated WBCs have to be made available so that one can quickly evaluate the amount of activity uptake and received dose for minimizing the effects of ionizing radiation to the human body. However, experimental data may be lacking and numerical simulations in the form of readily available models present a convenient tool for simulating the response of a detector. In recent years, increased computer power has led to many different designs of mathematical human phantoms, which can be used for Monte Carlo (MC) simulations of various measurement geometries [101].

The work that was performed up to this state of the task uses MC simulations of several radionuclide source distributions in a number of computational phantoms.

8.1 The IRINA phantom

8.1.1 Technical Data

The experimental unified phantom UPh-08T is referred to as IRINA and is made up of polyethylen (PE) blocks which can be assembled in ways as to represent

different sizes and geometries of the human body [102]. There are 6 sizes for the representation of different ages/sizes of humans for dose measurements, cf. Tab. 8.1.

Table 8.1: Sizes of the experimental unified phantom UPh-08T in terms of "number of PE blocks", "phantom mass" and what human size each geometry corresponds to "corresponding human size".

	number of PE blocks full-size / half	mass of assembled phantom [kg]	corresponding human size age and mass
P1	12	10.6	infant, 1 year, 12 kg
P2	21/6	20.9	child, 6 years, 24 kg
P3	36/28	42.9	teenager, 14 year, 50 kg
P4	69/2	61.5	adult, 70 kg
P5	72/36	77.8	adult, 90 kg
P6	90/40	95.2	adult, 110 kg

The phantoms in standing geometry are assembled according to Fig. 8.1 which, if examined properly, shows that there are two different sizes to the PE blocks (P5 as example with blocks in light-green, light-blue, blue and purple approximately half as thick as the others). Each PE block is traversed by two empty channels that are used for the insertion of rod radionuclide sources in order to model internal contamination through homogeneous or localized source distributions. That way, experimental calibration studies of WBCs are possible. However, only sources of ^{60}Co, ^{137}Cs and ^{40}K are provided by the UPh-08T and numerical simulations may be necessary when using the phantom with other sources.

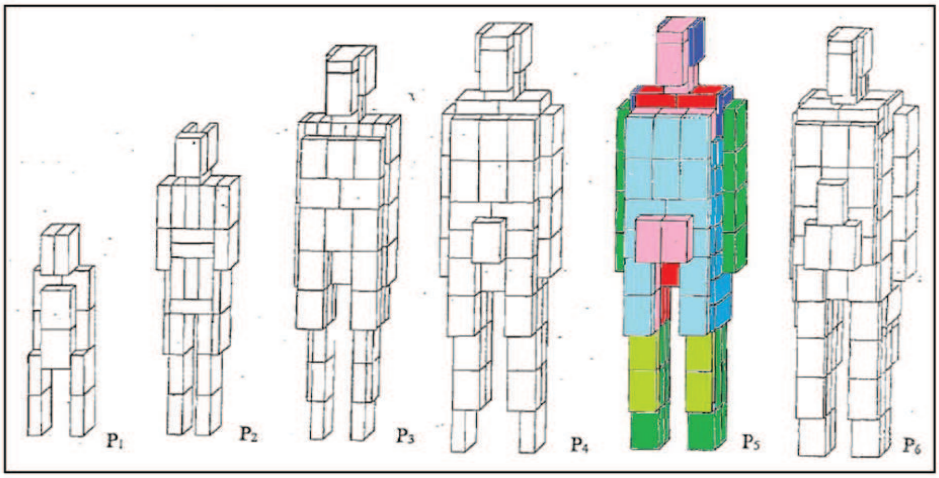

Figure 8.1: Drawing of standing geometry of the experimental unified phantom UPh-08T for all 6 sizes (P5 colored for clarification).

8.1.2 The IRINA voxel phantom

For the purpose of Monte Carlo simulations, a geometry-file of the modeled object has to be defined and thus, a so-called voxel phantom of the UPh-08T was programmed. The algorithm uses the technical computing language MATLAB® for programming all 6 sizes of the standing geometry of the UPh-08T and are called IRINA(-P1, -P2,..., -P6) voxel phantoms. The outcome of this procedure is shortly described in a letter to the editor of the Journal of Radiation Protection Dosimetry (paper VI) and detailed instructions on how to construct the IRINA voxel phantoms are given in paper VII.

General conclusions from the report to the Nordic Nuclear Safety Research (NKS) are the following:

- Since each MC code uses specific geometry definitions it is of interest to provide a code-independent structure of the voxel phantom. This was achieved with the provided IRINA voxel phantoms.
- Simulations with the Monte Carlo code GATEv7.0, cf. subsection 8.2.1, were made to test the validity of the simplifications used for modeling the geometry of a fully-sized PE block. The code was also used to verify the geometry of the IRINA voxel phantom by comparing the placement of source tubes (channel for insertion of rod radionuclide sources) and PE blocks in the MC model to the technical documentation of the experimental unified phantom UPh-08T.
- All 6 sizes of the standing geometry were successfully programmed in MATLAB® and are available through the NKS website.
- The voxel phantoms are defined in terms of material identification numbers (ID). Apart from material IDs for PE and air, each source tube has an individual material ID in order to allow for localized source distributions. For all IRINA voxel phantoms, maps over these individual material IDs are available through the NKS website.

8.2 Comparison of Phantoms

Whole-body counting is a well-established method to determine the activity of radioactive elements in the human body by analyzing the emitted gamma radiation. The measurements may be performed with the aim to check for possible internal contamination or to estimate an accidental intake of radionuclides. In its simplest form, this can be achieved by placing a radiation detector close to the body even if in reality, more advanced technology in the form of specialized shielded detector configurations is used.

Due to scattering in the body, the measurement signal will depend on the subject's size and a suitable calibration is necessary. Apart from the subject's

size and geometry, the distribution of the radionuclide within the body has an impact on the data analysis of such a measurement and if detector systems are calibrated for a homogeneous distribution, the uncertainty in the estimated activity will increase unless the biodistribution of the radionuclides is taken into account [103].

The following study aims at:

- performing MC simulations for the comparison of two voxel phantoms that describe the same experimental unified phantom UPh-08T with size P4;
- comparing the outcome of simulations using the computational version of the UPh-08T phantom (size P4) and the ICRP reference adult male voxel phantom;
- investigating the impact of biodistribution on the activity estimation by using ^{60}Co and ^{140}La which, with respect to their difference in biokinetic retention, are relevant examples of nuclides released in a nuclear accident.

8.2.1 Simulations

All simulations were done with the open-source software GATE[3] (version v7.0) [104] which uses the GEANT4 [105] physics libraries for simulations of medicine imaging and radiation therapy. Sources of ^{60}Co and ^{140}La were defined as ion sources and the radioactive decay mode was used.

To evaluate the differences between the voxel phantoms, the energy of the γ-photons incident on five cylindrical volumes were investigated with their size (radius 6.35 cm and height 5.0 cm) chosen in a way as to represent a medium-sized detector. The detector volumes are positioned according to source compartments, cf. 8.2.2. The simulations hence show how the energy of the incident γ-photons on a detector, if placed at a cylinder position, changes due to differences between the voxel phantoms.

8.2.2 IRINA vs. IGOR

Just like the IRINA voxel phantom, the IGOR voxel phantom (size P4 in standing geometry) is a virtual description of the experimental unified phantom UPh-08T [106, 107]. While the standing IRINA voxel phantoms were programmed in MATLAB®, the IGOR voxel phantom was created from a computer-tomographic (CT) scan of the assembled experimental phantom by segmentation of CT-images [108].

[3] **G**EANT4 **A**pplication for **T**omographic **E**mission

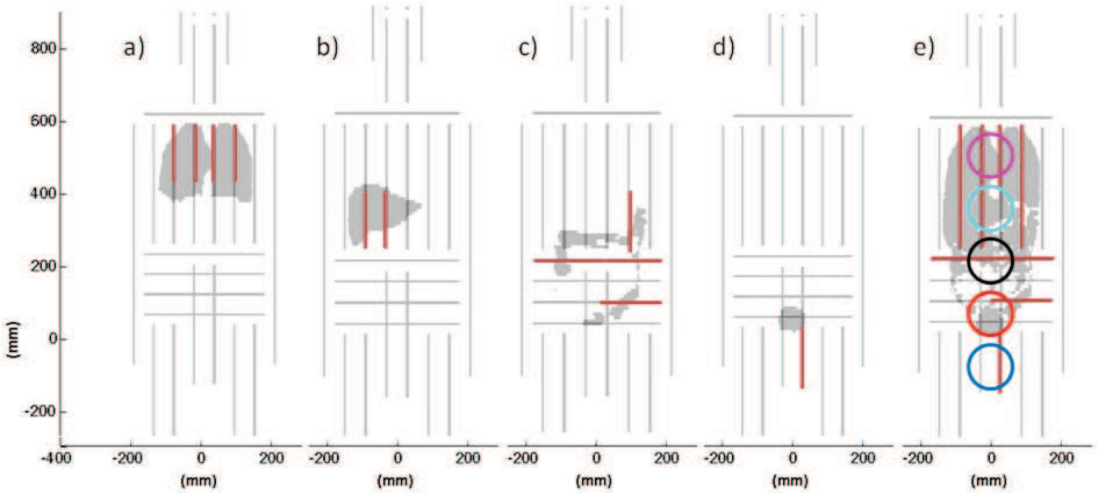

Figure 8.2: Illustration for the positioning of a) - d) organ compartments and e) detector volume positions used in Monte Carlo simulations with GATE. The compartments are: a) lungs, b) liver, c) intestines and d) urinary content. Grey-shaded compartments symbolize organs according to the ICRP reference adult male voxel phantom, red-bold lines represent rod radionuclide sources and grey lines are empty source tubes in the IRINA/IGOR voxel phantoms

Both voxel phantoms are differently parameterized in terms of voxel size and geometrical details, mostly concerning the amount of air-filled voxels within the PE blocks. In order to test and validate the performance of the IRINA voxel phantom, simulations for the comparison with the IGOR voxel phantom are made [109].

This task uses 4 localized source distributions of ^{60}Co in IRINA and IGOR for simulations with GATE. The compartments for the localization of sources symbolize the position of organs relevant to activity inhalation and ingestion, i.e. lungs, liver, intestines and urinary content [110]. For each source distribution, the energies from 10^7 decays of ^{60}Co are scored in all five detector volumes and out of these the energy spectrum with the highest total number of counts was chosen for the evaluation of the differences between the voxel phantoms. The total number of counts and the peak-to-total ratios for all localized source distributions in IRINA and IGOR are presented in Tab. 8.2.

The differences in total activity between IRINA and IGOR range between +0.1 and -0.4%. Thus, both approaches for creating voxel phantoms, i.e. the segmentation of CT-images and programming in MATLAB®, agree with each other and render similar results as these differences are on the same order of magnitude as the statistical error of 0.1%. The amount of un-scattered γ-particles, which is the peak-to-total ratio, is on average 2.6% larger in IGOR than in IRINA, cf. Tab. 8.2. This can be attributed to the methods and simplifications that are used to cre-

ate either voxel phantom: as explained in detail in papers VII and VIII, air-filled connector holes are filled with PE and gaps between blocks are not modeled in IRINA. Therefore, the scattering density is larger than in IGOR, which contains air in a manner as the experimental unified phantom does, so that the peak-to-total ratio in IRINA is smaller than in IGOR.

Table 8.2: Total number of counts incident on the most responsive detector volume and peak-to-total ratio for all organ distributions of ^{60}Co to compare IRINA and IGOR.

	compartment	IRINA	IGOR
Total counts incident on detector volume	**Lungs**	613694	614393
	difference		+ 0.11%
	Liver	621241	618607
	difference		- 0.42%
	Intestines content	620787	621320
	difference		+ 0.08%
	Urinary content	643108	641552
	difference		- 0.23%
Peak-to-total ratio $\gamma_1 + \gamma_2$	**Lungs**	0.54	0.56
	difference		+ 2.4%
	Liver	0.52	0.54
	difference		+ 2.9%
	Intestines content	0.58	0.56
	difference		+ 2.3%
	Urinary content	0.60	0.61
	difference		+ 2.7%

8.2.3 IRINA vs. ICRP

The ICRP reference adult male voxel phantom [111] serves as a standard for validating the simulations with the IRINA voxel phantom. Representing a human of length 176 cm and weight 73 kg, the measures of the ICRP reference adult male voxel phantom compare to the P4 geometry of the IRINA voxel phantom which is supposed to represent a 170.5 cm tall adult of weight 70 kg. The ICRP reference adult male voxel phantom was also used for assigning the position of the aforementioned 4 compartments, cf. Fig. 8.2.

Similar to the previous case, cf. subsection 8.2.2, 10^7 Bq of ^{60}Co were evenly distributed in all organ compartments and the whole-body. The results of the simulations with GATE are presented in Tab. 8.3. Here, the deviations between the voxel phantoms for the localized source distributions are on the order of 3% even though the organ geometries differ a lot from each other, cf. Fig. 8.2.

Interestingly, the number of counts incident on the detector volume for the whole-body distribution in the ICRP reference adult male voxel phantom is more than 10% smaller than in the IRINA voxel phantom. The reason for the discrepancies between the two phantoms is much likely attributed to their differences in size and geometry: the IRINA voxel phantom is not only 5.5 cm shorter and has a larger upper body than the ICRP reference adult male voxel phantom, but also the true mass of the experimental unified phantom in P4 standing geometry differs by 11.5kg from the ICRP reference adult male voxel phantom and is thus 15.8% lighter, cf. Tab. 8.1. As a result of this, the densities of the phantoms but also the amount of other tissue between source and detector volume are different for the two phantoms so that fewer particles are scattered by the IRINA voxel phantom, leading to a higher number of counts incident on the detector volume.

The performed simulations helped to quantify the differences between the phantoms and may be useful for comparisons towards experimental results.

Table 8.3: Total number of counts incident on the most responsive detector volume for whole-body and all organ distributions of ^{60}Co to compare IRINA and ICRP.

	compartment	IRINA	IGOR
Total counts incident on detector volume	**Whole-body**	272907	235769
	difference		-13.6%
	Lungs	613694	618140
	difference		+ 0.72%
	Liver	621241	599608
	difference		- 3.62%
	Intestines content	620787	609318
	difference		- 1.85%
	Urinary content	643108	625750
	difference		- 2.69%

8.2.4 Effect of biodistribution on WBC calibration

In an emergency situation it may be necessary to quickly estimate the amount of activity of a contaminated individual and whole-body counting is commonly applied in that respect. However, the uncertainty of such measurement results depends on the calibration of the system which in turn may vary in accordance to its setup and geometry. The following study simulates a realistic distribution of ^{140}La [112] in the human body and shows how the amount of incident photons on a detector volume compares to a whole-body source distribution such as often used for system calibrations.

Simulations of 10^7 Bq of ^{140}La concentrated in the liver and distributed throughout the human body are performed with the IRINA-P4 voxel phantom and the ICRP reference adult male voxel phantom. As previously, only the detector volume with the largest sum of incident particles was used for the data analysis. The normalized energy spectra for the two distributions are used to compare both voxel phantoms and are given by Fig. 8.3. In the case of the whole-body simulation, both phantoms render more or less the same spectrum shape. When all activity is contained within the liver compartment, it is seen that the gamma particles scatter less in IRINA than in ICRP since for IRINA, the peak-to-total ratio is higher than for ICRP.

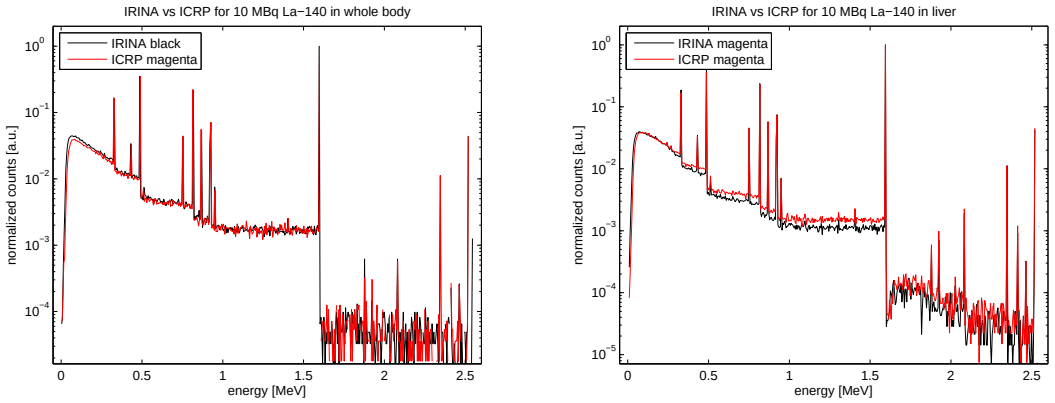

Figure 8.3: Normalized energy spectrum for ^{140}La in whole-body and liver for the comparison of IRINA and ICRP.

The biokinetic model for ^{140}La indicates that 60% of the activity in the human body upon uptake in blood accumulates in the liver while the remaining 40% are distributed throughout the whole-body [113]. For determining the total activity received after the uptake of any radioisotope, it is necessary to calculate its retention over time which for the case of ^{140}La in the liver is a combined function of two exponentials that use the specific biological and physical half-lifes. Weighing the simulated energy spectra, according to this biokinetic model, results in Fig. 8.4. It is then observed that the spectrum of the 60/40 source distribution exhibits a higher number of counts than the whole-body distribution.

These differences are calculated and summarized in Tab. 8.4, showing the average ratio between the two cases for a number of relevant energy regions. For simulations with IRINA, the ratio decreases from around 1.7 to 1.5 for the intervals. A similar trend but of higher magnitude is observed for the γ-lines, i.e. from more than 2 to 1.8. Here, an energy-dependence is observed which may be of interest when measurement setups are sensitive to energy. For simulations with the ICRP reference adult male voxel phantom, the ratio between the two distributions is approximately constant at 1.85.

Conclusively, the results quantify the differences between homogeneous and localized source distributions for different phantoms and may be helpful when comparisons towards experiments shall be made.

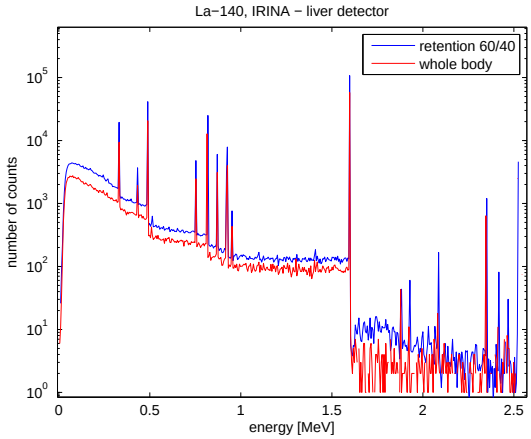

Figure 8.4: Energy spectrum for ^{140}La for IRINA to compare whole-body vs. maximum retention in liver.

Table 8.4: Ratio between spectra of the 60/40 retention and whole-body distributions for detector volume in height with the liver for significant energy intervals for simulations with IRINA and ICRP.

Energy [MeV]	IRINA	ICRP
0.03 - 0.32	1.72	1.88
γ_1 = 0.328	2.07	1.85
0.33 - 0.48	1.56	1.83
γ_2 = 0.487	2.01	1.90
0.49 - 0.81	1.47	1.74
γ_3 = 0.815	1.96	1.89
0.82 - 1.59	1.46	1.74
γ_4 = 1.596	1.86	1.84
γ_5 = 2.521	1.84	1.91

CHAPTER

9

Summary

9.1 Part I - Material Research

The Chalmers Pulsed Positron Beam was calibrated by expressing the positron penetration depth as a function of high-voltage positron acceleration. Experimental and calculated depth profiles show that the point of annihilation within a metallic lattice moves by approximately 20 nm per keV. This information is interesting for investigations concerning the depth of lattice defects that may be created by means of irradiation procedures.

For the simulation of neutron-induced radiation damage, the international GETMAT and the national GENIUS project use self-ion irradiation experiments. The mechanisms of damage production with either neutrons or ions differ substantially from each other but the advantages of ion-irradiation procedures strongly motivate the development of theoretical and experimental models for the emulation of neutron-damage with ions. PALS is used a very sensitive tool for the investigation of vacancy-type radiation-induced material damage and it was shown that the micro-structural material properties are governed by a number of processes directly related to the irradiation procedure. Here, irradiation dose and temperature appear to be coupled in a difficult manner which within GETMAT is strongly related to the irradiation/heating time. Kinematic effects like defect migration and recombination were observed when changing the order of ion-energy. The involvement within GETMAT and GENIUS was aimed at studying the radiation resistance of FeCr alloys of varying chemical composition. With respect to that, our conclusions were not successful. Instead it was shown that the formation of large voids or other positron-sensitive structures such as dislocation loops are strongly influenced by the parameters of the irra-

diation procedure. For reliable conclusions on experimental defect mechanisms with slow positrons it is thus of stressed, that the number of variables in an irradiation experiment should be kept small since phenomena regarding the kinetics of lattice defects are coupled in a complicated manner.

9.2 Part II - Nuclear Safeguards and Emergency Preparedness

Different detection techniques were successfully applied for measurements relevant to the research field of safeguards.

With the help of Pulse Shape Discrimination upon data obtained from liquid scintillator detectors it was shown that the presence of B in water changes the shape of the signal due to large variations in the γ energies resulting from the absorption of neutrons in the relevant isotopes B and H. This information can be used to estimate the amount of B in water which in turn can be applied as a correction factor to imaging techniques used for the evaluation of the content in a facility for the storage of spent fuel.

The liquid scintillator of type EJ-309 was also used for confirming measurements of neutrons released from a strong ^{241}Am source. High-resolution energy spectra as obtained by a HPGe detector were evaluated and could be used for the characterization of source-inherent impurities. Impurities may be important signatures for the archival storage of source properties and other relevant data in national libraries which are stipulated by the IAEA for quick and simplified access to information necessary for nuclear forensics or orphan source investigations.

Work within the field of emergency preparedness was performed on base of Monte Carlo simulations. Estimations on the received dose in case of an emergency often use activity measurements which may lack accuracy due to the measurement setup and geometry as well as the distribution of a radioactive source within the human body. The simulations use geometry files, referred to as voxel phantoms, that differ in parametrization. While the ICRP reference adult male voxel phantom is based on real human data, the IGOR and IRINA phantoms are virtual descriptions of the UPh-08T unified phantom and were obtained by either CT-image segmentation or numerical programming, respectively. All voxel phantoms were compared towards each other and showed good agreement. Thus, the algorithm for the programming of the IRINA voxel phantom could be proven valid and, due to its benefits of being general, simple and fast, the IRINA voxel phantom should be used for WBC calibration purposes. It was also presented, that distributions of ^{140}La on base of its biokinetic retention alter the activity estimation and, if applicable, isotope-specific processes should be regarded for the correct calibration of activity and dose measurement setups.

9.3 Outlook

There are a number of different ideas on how to develop the findings of the presented research.

For the increased accuracy of lifetime measurements with the available PALS equipment and thus, further defect studies, a number of modifications to the Chalmers pulsed positron beam would be advantageous:

- For more efficient and statistically relevant PALS measurements, the positron source might be exchanged since the present ^{22}Na source is older than 3 half-lifes which reduces the number of emitted positrons in comparison to the time when the measurements were performed in the first place.

- Crucial for an increased time-resolution of the annihilation lifetime spectrum is the design of the chopper/buncher system which ideally should produce mono-energetic positron pulses. It is primarily the chopper that controls the properties of the pulse and advancements regarding the operation frequency and signal shape (sine vs. rectangular) would have a beneficial impact on the time-resolution.

- Other ideas for increasing the performance of the Chalmers pulsed positron beam relate to increasing the trapping probability by sample cooling and further increase in time resolution by using a digitalized data acquisition system as discussed for positron beam advances [114–116].

With regard to the performed depth profiling for the calibration of the Chalmers pulsed positron beam, it would be of great value to use the Au-layered samples measurements in similar beam laboratories for the validation of our findings from experiment and simulation.

Concerning defect studies with the help of positron annihilation, it should be emphasized that ion-irradiation experiments for the simulation of neutron damage have to be performed under detailed control of irradiation conditions such as temperature exposure and/or time. For a deep understanding of experiments on radiation-induced lattice defects one would like to use pure elements in order to keep the number of variable parameters low.

Ideas for the future of the work presented in the second part of the thesis are as follows:

The proposed method on the independent evaluation of the B content in water has evolved into new approaches to the issue and is studied further for future applications [117].

Information on source impurities may be implemented within national libraries and used as complementary signatures for the identification of sources in national libraries.

Lastly, the project related to simulations with IRINA is supposed to be continued in the form of real WBC measurements and calibrations by using the experimental unified phantom UPh-08T and subsequent comparisons to simulations of the setup. A number of different sources and distributions according to their biokinetic retention should be used.

Acknowledgements

Finishing this thesis took a bit longer than expected...

Thank you Anders Nordlund, for all your patient supervision, inspiration and support on a professional as well as personal basis. I appreciate the time you took to discuss any kind of topic and working together in the lab was very educational. You encouraged me to continue when I felt de-motivated and doubtful about my research and even if it may appear natural to you, I am grateful for all the respect and understanding I received during two periods of parental leave.

I would like to thank my co-supervisor Prof. Imre Pazsit for helping to form the thesis and for supporting my ideas. Your engagement to academia is truly inspiring and I am glad to have worked with you since I was a MSc student.

My co-supervisor Prof. Dina Chernikova is acknowledged for introducing me to the field of Nuclear Safeguards and Security and for including me into the group. Thank you for a challenging and interesting co-operation with you and parts of the group: Kåre Axell, Anna Vesterlund and Henrik Ramebäck.

I do not only thank Prof. Mats Isaksson for being my co-supervisor in the latter stages of my research but also for deepening my interest in radiation physics and protection through a number of inspiring lectures. Thank you for the opportunity of working together with you and Dr. Jenny Nilsson.

Prof. Christophe Demaziere, your support and interest in my work is highly appreciated. Most of all, I want to thank you for my first lecture on Reactor Physics in September 2006 which marks the start of my favorite topic: nuclear power.

This PhD work was financially supported by the Swedish Centre for Nuclear Technology (SKC), the GETMAT project as part of the 7th EURATOM framework programme of the European Commission and the GENIUS projected supported by the Swedish Research Council (Vetenskapsrådet), which is gratefully acknowledged.

I would like to thank Prof. Janne Wallenius and Prof. Christian Ekberg for all the irregular occasions to talk about science and, moreover, other stuff. Additional thanks for sharing your knowledge with me are directed towards: Lorenzo Malerba, Mercedes ”Merche” Hernández-Mayoral, Frank Bergner and Cornelia ”Conny” Heintze; Mattias Thuvander and Jesper Ejenstam; Adam Balogh, Pär Olsson and Paul Erhart.

As a board member of the Swedish Young Generation Network and the IYNC I got to make many valuable friendships and to experience the diversity of the nuclear industry. Thank you all for the opportunity!

I am sorry to admit that I cannot count how many colleagues and room mates I had during my years at the Department for Nuclear Engineering but I know that all of you - past, present and occasional - contributed to an interesting work environment that I will bear in mind forever.

Thanks to all my friends and family for supporting me! Your curiousness motivates me to seek a deeper understanding and simpler explanations.

My greatest appreciation is directed towards the people I love most on this planet:
My beloved parents...
Because of you believing in me at all times, I am where I am today!

Henrik...
You turned my life into ours!
We gave each other a meaning in life that is bigger than what we ever imagined.
I know no words or actions that can express how grateful I am for our family.
Thank you for being you (and mine)!

Alicia and Amelie...
I dedicate this work to you...
I love you to the end of the universe!

REFERENCES

[1] The Oxford Dictionary, www.oxforddictionaries.com/definition/ english/radiation, 2015.

[2] Nobel Media AB, *The Nobel Prize in Physics 1903*, www.nobelprize.org/nobel_prizes/physics/laureates/1903, 2014.

[3] Brookhaven National Laboratory - National Nuclear Data Center, *Chart of Nuclides*, https://commons.wikimedia.org/wiki/File:Nuclide Map_stitched.png, 2008.

[4] United Nations Scientific Committee, *Sources and Effects of Ionizing Radiation*, www.unscear.org/docs/reports/2008/11-80076_Report_ 2008_Annex_D.pdf, 2008.

[5] ICRP-103, "The 2007 recommendations of the international commission on radiological protection," *Annals of the ICRP*, vol. 37, no. 2-4, 2007.

[6] C. McEvedy and R. Jones, *Atlas of World Population History*. Penguin, 1978.

[7] United Nations: Department of Economic and Social Affairs - Population Division, *World Population Prospects - The 2015 Revision: Key Findings and Advance Tables*, http://esa.un.org/unpd/wpp/Publications/ Files/Key_Findings_WPP_2015.pdf, 2015.

[8] J. Cook *et al.*, "Quantifying the consensus on anthropogenic global warming in the scientific literature," *Environmental Research Letters*, vol. 8, no. 2, 2013.

[9] W. Moomaw, F. Yamba, *et al.*, *Renewable Energy and Climate Change*, chapter in: Renewable Energy Sources and Climate Change Mitigation. IPCC Special Report, Cambridge University Press, 2011.

[10] www.worldcoal.org, July 2014.

[11] J. Sathaye, O. Lucon, A. Rahman, *et al.*, *Renewable Energy in the Context of Sustainable Development*, chapter in: Renewable Energy Sources and Climate Change Mitigation. IPCC Special Report, Cambridge University Press, 2011.

[12] H. Nifenecker, *The Energy Issue and the Possible Contribution of the Various Nuclear Energy Production Scenarios*, chapter in: Materials Issues for Generation IV Systems. NATO Science for Peace and Security Series B: Physics and Biophysics, Springer, Netherlands, 2008.

[13] IAEA, *Nuclear Power Reactors in the World 2015 Edition*, http://www-pub.iaea.org/books/, 2015.

[14] OECD Nuclear Energy Agency, *Technology Roadmap Update for Generation IV Nuclear Energy Systems*, https://www.gen-4.org/, 2014.

[15] F. Carré, C. Renault, P. Anzieu, P. Brossard, and P. Yvon, *Outlook on Generation IV Nuclear Systems and Related Materials RD Challenges*, chapter in: Materials Issues for Generation IV Systems. NATO Science for Peace and Security Series B: Physics and Biophysics, Springer, Netherlands, 2008.

[16] IAEA, Austria, *Development of Radiation Resistant Reactor Core Structural Materials - NTR2007 Supplement*, Information Documents to the 51st General Conference, 2007.

[17] K. E. Holbert, *Radiation Effects and Damage*, Lecture notes from EEE 598. School of Electrical, Computer and Energy Engineering, Arizona State University, 2008.

[18] S. J. Zinkle, *Microstructures and Mechanical Properties of Irradiated Metals and Alloys*, chapter in: Materials Issues for Generation IV Systems. NATO Science for Peace and Security Series B: Physics and Biophysics, Springer, Netherlands, 2008.

[19] T. R. Allen, *High Dose Radiation Effects in Steels*, chapter in: Radiation Effects in Solids. NATO Science Series, Springer, Netherlands, 2007.

[20] S. J. Zinkle, *Impact of Radiation Damage on Materials for Nuclear Energy Systems*, Lecture notes. EFRC Summer School on Defects, Deformation and Damage in Structural Materials, ORNL, Knoxville - US, 2012.

[21] R. A. Knief, *Nuclear energy technology: theory and practice of commercial nuclear power*. McGraw-Hill, Hemisphere Publishing Corporation, Washington DC, 1981.

[22] M. Ragheb, *Transport and Diffusion Reactor Theory - Neutron Collision Theory*, Lecture notes from NPRE 402 ME 405 Nuclear Power Engineering. Department of Nuclear, Plasma and Radiological Engineering, University of Illinois, 2006.

[23] K. A. Assamagan, *Nuclear Physics - lecture 26*, Lecture notes. Second Biennial African School on Fundamental Physics and its Applications, Kumasi, Ghana, 2012.

[24] G. S. Was, *Fundamentals of Radiation Materials Science: Metals and Alloys*. Springer, Berlin Heidelberg, 2007.

[25] J. Koutsky and J. Kocik, "Radiation damage of structural materials," *Materials Science Monographs*, vol. 79, pp. 3–361, 1994.

[26] H. Föll, "Defects in crystals." http://www.tf.uni-kiel.de/matwis/amat/def_en/, 1976.

[27] K. L. Murty, *Radiation Damage*, Lecture notes from NE 409/509. Department of Material Science Engineering - Nuclear Engineering, North Carolina State University, 2004.

[28] R. M. Mayer, "Nucleation and growth of voids by radiation: VII. correlation of charged particle and neutron irradiations," *Journal of Nuclear Materials*, vol. 95, no. 1-2, pp. 100–107, 1980.

[29] M. Li, *Moving from DPA to changes in material properties*, Lecture notes to the session on "Modeling Radiation Effects in Magnets and Material Response". Workshop on Radiation Effects in Superconducting Magnet Materials, Fermilab, Chicago-US, 2012.

[30] J. F. Ziegler, M. D. Ziegler, and J. P. Biersack, "SRIM - the stopping and range of ions in matter," *Nuclear Instruments and Methods in Physics Research B*, vol. 268, no. 11-12, pp. 1818–1823, 2010.

[31] R. E. Stoller, M. B. Toloczko, G. S. Was, A. G. Certain, S. Dwaraknath, and F. A. Garner, "On the use of SRIM for computing radiation damage exposure," *Nuclear Instruments and Methods in Physics Research B*, vol. 310, pp. 75–80, 2013.

[32] R. Stoller, *Introduction to Radiation Damage Mechanisms*, Lecture notes. EFRC Summer School on Defects, Deformation and Damage in Structural Materials, ORNL, Knoxville - US, 2012.

[33] J. O. Stiegler, ed., *Proceedings of the Workshop on Correlation of Neutron and Charged Particle Damage*. ORNL, 1976.

[34] L. K. Mansur, "Correlation of neutron and heavy-ion damage: II. The predicted temperature shift if swelling with changes in radiation dose rate," *Journal of Nuclear Materials*, vol. 78, no. 1, pp. 156–160, 1978.

[35] C. Abromeit, "Aspects of simulation of neutron damage by ion irradiation," *Journal of Nuclear Materials*, vol. 216, pp. 78–96, 1994.

[36] G. S. Was and R. S. Averback, *Radiation Damage using Ion Beams*, chapter in: Comprehensive Nuclear Materials: Five Volume Set. Newnes, 2011.

[37] G. S. Was, Z. Jiao, E. Getto, K. Sun, A. M. Monterrosa, S. A. Maloy, O. Anderoglu, B. H. Sencer, and M. Hackett, "Emulation of reactor irradiation damage using ion beams," *Scripta Materialia*, vol. 88, pp. 33–36, 2014.

[38] G. S. Was, "Challenges to the use of ion irradiation for emulating reactor irradiation," *Journal of Materials Research*, vol. 30, no. 9, pp. 1158–1182, 2015.

[39] G. S. Was and T. R. Allen, *Radiation Damage from Different Particle Types*, chapter in: Radiation Effects in Solids. NATO Science Series, Springer, Netherlands, 2007.

[40] R. S. Averback and P. Bellon, *Fundamental Concepts of Ion-Beam Processing*, chapter in: Materials Science with Ion Beams. Topics in Applied Physics, Springer, Berlin Heidelberg, 2010.

[41] R. S. Averback, "Ion-irradiation studies of cascade damage in metals," *Journal of Nuclear Materials*, vol. 108 109, pp. 33–45, 1982.

[42] H. Wiedersich, "Effects of the primary recoil spectrum on long-range migration of defects," *Radiation Effects and Defects in Solids*, vol. 113, pp. 97–107, 1990.

[43] M. E. G. Valerio, *Defeitos associados a feixe de particulas energeticas*, Lecture notes. Federal University of Sergipe - Physics Department, Brazil, 2011.

[44] R. S. Averback, "Atomic displacement processes in irradiated metals," *Journal of Nuclear Materials*, vol. 216, p. 49, 1994.

[45] K. E. Sickafus, E. A. Kotomin, and B. P. Uberuaga, eds., *Radiation Effects in Solids*, vol. 235 of *NATO Science Series*. Springer, 2007.

[46] H. Lyle, *Oral History Project - Interview with Carl D. Anderson*, retrieved 2014-07-09 from: http://resolver.caltech.edu/CaltechOH:OH_Anderson_C. California Institute of Technology Archives, 1979.

[47] C. D. Anderson, "The apparent existence of easily deflectable positives," *Science*, vol. 76, pp. 238–239, 1932.

[48] P. A. M. Dirac, "The quantum theory of the electron," *Proceedings of the Royal Society of London A*, vol. 117, no. 778, pp. 610–624, 1928. doi: 10.1098/rspa.1928.0023.

[49] P. A. M. Dirac, "A theory of electrons and protona," *Proceedings of the Royal Society of London A*, vol. 126, no. 801, pp. 360–365, 1930. doi: 10.1098/rspa.1930.0013.

[50] P. A. M. Dirac, "Quantised singularities in the electromagnetic field," *Proceedings of the Royal Society of London A*, vol. 133, no. 821, pp. 60–72, 1931. doi: 10.1098/rspa.1931.0130.

[51] C. D. Anderson, "The positive electron," *Physical Review*, vol. 43, pp. 491–498, 1933.

[52] Nobel Media AB, "The Nobel Prize in Physics 1936 - Carl. D. Anderson." www.nobelprize.org/nobel_prizes/physics/laureates/1936/anderson-facts.html, 2014.

[53] Nobel Media AB, "The Nobel Prize in chemistry 1935." www.nobelprize.org/nobel_prizes/chemistry/laureates/1935/, 2014.

[54] T. M. Hall, A. N. Goland, and C. L. S. Jr., "Applications of positron-lifetime measurements to the study of defects in metals," *Physical Review B*, vol. 10, no. 8, 1974.

[55] University of Michigan - Michigan NanoPos group, "PALS tutorial." http://positrons.physics.lsa.umich.edu/current/nanopos/PALS-intro/index.htm, 2015.

[56] A. F. Makhov, "The penetration of electrons into solids," *Soviet Physics Solid State 2*, p. 1945 ff., 1960.

[57] R. Krause-Rehberg and H. S. Leipner, *Positron Annihilation in Semiconductors*. Springer, 1999.

[58] J. Dryzek. http://www.ifj.edu.pl/mdryzek/page_h1.html, 2015.

[59] S. van Petegem, C. Dauwe, T. van Hoecke, J. de Baerdemaeker, and D. Segers, "Diffusion length of positrons and positronium investigated using a positronbeam with longitudinal geometry," *Physical Review B*, vol. 70, 2004.

[60] P. Hautojärvi and C. Corbel, *Positron Spectroscopy of Defects in Metals and Semiconductors*, chapter in: Proceedings of the International School of Physics "Enrico Fermi" - Positron Spectroscopy in Solids. IOS Press, 1995.

[61] A. Seeger, "Positron diffusion in solids and in liquid metals," *Applied Surface Science*, vol. 85, pp. 8–16, 1995.

[62] M. Charlton and J. W. Humbertson, *Positron Physics*. Cambridge University Press, Cambridge, 2001.

[63] R. M. Nieminen, *Electronic Structure and Positron Spectroscopy of Solids and Surfaces*, chapter in: Proceedings of the International School of Physics "Enrico Fermi" - Positron Spectroscopy in Solids. IOS Press, 1995.

[64] J. M. C. Robles, E. Ogando, and F. Plazaola, "Positron lifetime calculation for the elements of the periodic table," *Journal of Physics: Condensed Matter*, vol. 19, 2007.

[65] R. Krause-Rehberg, *Fundamentals of positron annihilation spectroscopy and its application in semiconductors*, Lecture notes from 15th International Conference on Positron Annihilation. Martin-Luther University Halle-Wittenberg, India, 2009.

[66] http://www.positronannihilation.net/index.htm, 2014.

[67] J. D. Baerdemaeker, *Defect Characterization of sputtered, nitrided and ion implanted materials using the Ghent slow positron facility*. PhD thesis, Ghent University, 2004.

[68] L. Mileshina and A. Nordlund, "Design and performance of the pulsed positron beam at chalmers university of technology," *Nuclear Instruments and Methods in Physics Research B*, vol. 267, pp. 2934–2937, 2009.

[69] M. Galan, *LNE - LNHB/CEA Table de Radionuclides - Na-22 (vol. 5)*, www.nucleide.org/DDEP_WG/Nuclides/Na-22_tables.pdf. CIEMAT, 2009.

[70] J. Kansy, "Microcomputer program for analysis of positron annihilation lifetime spectra," *Nuclear Instruments and Methods in Physics Research A*, vol. 374, no. 2, 1996.

[71] D. Giebel and J. Kansy, "A new version of LT program for positron lifetime spectra analysis," *Materials Science Forum*, vol. 666, pp. 138–141, 2011.

[72] J. Dryzek and J. Kansy, "Comparison of three programs: Positronfit, Resolution and LT used for deconvolution of positron lifetime spectra," *Nuclear Instruments and Methods in Physics Research A*, vol. 380, no. 3, 1996.

[73] J. Kansy and D. Giebel, "Study of defect structure with new software for numerical analysis of PAL spectra," *Journal of Physics: Conference Series*, vol. 265, 2011. International Workshop on Positron Studies of Defects.

[74] J. Kansy, *LT version9.0 electronic manual*. Institute of Physics, Silesian University, Katowice.

[75] F. Salvat, J. M. Fernandez-Varea, and J. Sempau, *PENELOPE-2008: A Code System for Monte Carlo Simulation of Electron and Photon Transport*, workshop proceedings. NEA, Barcelona, 2009.

[76] J. M. Fernandez-Varea. personal communication: PENELOPE, 2009.

[77] S. L. Dudarev, J.-L. Boutard, *et al.*, "The EU programme for modelling radiation effects in fusion reactor materials: An overview of recent advances and future goals," *Journal of Nuclear Materials*, vol. 386-388, 2009. Proceedings of the 13th International Conference on Fusion Reactor Materials.

[78] L. Malerba, A. Caro, and J. Wallenius, "Multiscale modelling of radiation damage and phase transformations: The challenge of FeCr alloys," *Journal of Nuclear Materials*, vol. 382, 2008. Proceedings of the Symposium on Microstructural Processes in Irradiated Materials, as part of the Annual Meeting of The Minerals, Metals Materials Society.

[79] M. Hernández-Mayoral, V. Kuksenko, C. Pareige, P. Pareige, P. Desgardin, B. Décamps, M. F. Barthe, A. Nordlund, P. Cartemo, A. Idhil, C. Borca, and C. Heintze, *Deliverable D 4.7: Microstructure and microchemistry characterisation of ion-irradiated FeCr alloys (concentration, dose and temperature): TEM, PAS, APT and Synchrotron techniques*, final internal report of the GETMAT project WP4. EC - 7th Euratom Framework Programme, 2013.

[80] C. Heintze *et al.*, "Ion-irradiation-induced damage of steels characterized by means of nanoindention," *Nuclear Instruments and Methods in Physics Research B*, vol. 267, pp. 1505–1508, 2009.

[81] M. J. Puska and R. M. Nieminen, "Defect spectroscopy with positrons: a general calculational method," *Journal of Physics F: Metal Physics*, vol. 13, no. 2, p. 342, 1983.

[82] J. Wallenius, *GENIUS & The Swedish Fast Reactor programme*, presentation from 45th Annual Meeting of the Technical Working Group on Fast Reactors (TWG-FR). IAEA, 2012.

[83] J. Wallenius, E. Suvdantsetseg, and A. Fokau, "ELECTRA: European lead-cooled training reactor," *Nuclear Technology*, vol. 177, no. 3, pp. 303–313, 2012.

[84] S. Bortot, J. Ejenstam, M. Pukari, E. Suvdantsetseg, P. Szakalos, and J. Wallenius, *European LEad-Cooled TRAining reactor: structural materials and design issues*, presentation from Technical Meeting on Liquid Metal Reactor Concepts: Core Design and Structural Materials. IAEA, 2013.

[85] P. Cartemo and A. Nordlund, *Positron lifetime measurements of irradiated Fe and FeCr alloy samples*, internal report for GENIUS, WP2, 2013.

[86] J. Ejenstam, *Corrosion resistant alumina-forming aloys for lead-cooled reactors*. PhD thesis, Kungliga Tekniska Högskola - Chemical Science and Engineering - Department of Surface and Corrosion Science, Stockholm, Sweden, 2015.

[87] J. Ejenstam, M. Halvarsson, J. Weidow, B. Jönsson, and P. Szakalos, "Oxidation studies of Fe10CrAl-RE alloys exposed to pb at 550° C for 10,000 h," *Journal of Nuclear Materials*, vol. 443, no. 1-3, pp. 161–170, 2013.

[88] https://www.iaea.org/about/history, 2015.

[89] B. Sanders, "A short history of nuclear non-proliferation," *Nuclear Law Bulletin*, no. 62, 1998. EC/IAEA/NEA.

[90] UN, *Background Information - History of the Treaty*, 2005 Review Conference of the Parties to the Treaty on the Non-Proliferation of Nuclear Weapons (NPT); www.un.org/en/conf/npt/2005/index.html, 2005.

[91] UN: Department for Disarmament Affairs, *The treaty on the non-proliferation of nuclear weapons (NPT)*, www.un.org/en/conf/npt/2005/npttreaty.html, 2000.

[92] A. Enqvist, *Safeguards: Modelling of the Detection and Characterization of Nuclear Materials*. PhD thesis, Chalmers Tekniska Högskola - Department of Applied Physics - Nuclear Engineering, Gothenburg, Sweden, 2010.

[93] http://www.atomicheritage.org/event/december-8-1953, 1953.

[94] http://ommsb.msb.se/main, 2015.

[95] F. N. Flakus, "Detecting and measuring ionizing radiation - a short history," *IAEA Bulletin*, vol. 23, no. 4, 1981.

[96] M. L'Annunziata, *Handbook of Radioactivity Analysis*. Academic Press, 2012.

[97] G. F. Knoll, *Radiation Detection and Measurement*. John Wiley Sons Inc., 2000.

[98] D. Chernikova, K. Axell, I. Pázsit, A. Nordlund, and R. Sarwar, "A direct method for evaluating the concentration of boric acid in a fuel pool using scintillation detectors for joint-multicipality measurements," *Nuclear Instruments and Methods in Physics Research A*, vol. 714, pp. 90–97, 2013.

[99] IAEA, Austria, *The Code of Conduct on the Safety and Security of Radioactive Substances*, http://www-ns.iaea.org/tech-areas/radiation-safety/code-of-conduct.asp, 2004.

[100] V. P. Chechev and N. K. Kusmenko, *LNE - LNHB/CEA Table of Radionuclides - Am-241 (vol. 5)*, www.nucleide.org/DDEP_WG/Nuclides/Am-241_tables.pdf. KRI, 2010.

[101] J. Nilsson, *Modeling of Radiative Processen in Organic Scintillators*. PhD thesis, University of Gothenburg - Department of Physics - Radiation Physics, Gothenburg, Sweden, 2014.

[102] Scientific Research Institute for Industrial and Sea Hygiene, Russia, *Technical documents for human whole body phantoms with reference samples of radionuclides potassium-40, cobalt-60 and caesium-137 - set-up UPh-08T*, technical description, 1996.

[103] G. H. Kramer, L. C. Burns, and S. Guerriere, "Monte Carlo simulation of a scanning detector whole body counter and the effect of BOMAB phantom size on the calibration," *Health Physics*, vol. 83, no. 4, pp. 526–533, 2002.

[104] S. Jan, G. Santin, D. Strul, S. Staelens, K. Assie, D. Autret, *et al.*, "GATE: a simulation toolkit for PET and SPECT," *Physics in Medicine and Biology*, vol. 49, no. 19, pp. 4543–4561, 2004.

[105] K. Amako, J. Apostolakis, H. Araujo, P. A. Dubois, M. Asai, G. Barrand, *et al.*, "Geant4 developments and applications," *IEEE Transactions on Nuclear Science*, vol. 53, no. 1, pp. 270–278, 2006.

[106] L. de Carlan, P. Roch, E. Blanchardon, and D. Franck, "New method of voxel phantom creation: application for whole-body counting calibration and perspectives in individual internal dose assessment," *Radiation Protection Dosimetry*, vol. 116, no. 1-4, pp. 160–164, 2005.

[107] L. de Carlan, P. Roch, E. Blanchardon, and D. Franck, "Application of voxel phantoms in whole-body counting for the validation of calibration phantoms and the assessment of uncertainties," *Radiation Protection Dosimetry*, vol. 125, no. 1-4, pp. 477–482, 2007.

[108] D. Franck, L. de Carlan, N. Pierrat, D. Broggio, and S. Lamart, "OEDIPE: a new graphical user interface for fast construction of numerical phantoms and MCNP calculations," *Radiation Protection Dosimetry*, vol. 127, no. 1-4, pp. 262–265, 2007.

[109] D. Broggio. personal communication: IGOR phantom, 2014.

[110] ICRP-67, "Age-dependent doses to member of the public from intake of radionuclides part 2: Ingestion dose coefficients," *Annals of the ICRP*, vol. 23, no. 3, 1993.

[111] ICRP-110, "Adult reference computational phantoms," *Annals of the ICRP*, vol. 39, no. 2, 2009.

[112] R. G. Helmer, *LNE - LNHB/CEA Table of Radionuclides - La-140 (vol. 1)*, www.nucleide.org/DDEP_WG/Nuclides/La-140_tables.pdf. INEEL, 2004.

[113] ICRP-30, "Limits for intakes of radionuclides by workers part 3," *Annals of the ICRP*, vol. 6, no. 2, 1981.

[114] K. Rytsölä, J. Nissilä, J. Kokkonen, A. Laakso, R. Aavikko, and K. Saarinen, "Digital measurement of positron lifetime," *Applied Surface Science*, vol. 194, no. 1-4, pp. 260–263, 2002.

[115] F. Becvar, J. Cizek, I. Prochazka, and J. Janotova, "The asset of ultra-fast digitizers for postiron-lifetime spectroscopy," *Nuclear Instruments and Methods in Physics Research A*, vol. 539, pp. 372–385, 2005.

[116] R. Aavikko, *Positron Lifetime Spectroscopy: Digital Spectrometer and Experiments in SiC*. PhD thesis, Aalto University - Department of Engineering Physics and Mathematics, Helsinki, Finland, 2006.

[117] D. Chernikova, S. F. Naeem, N. Trnjanin, K. Axell, and A. Nordlund, "Gamma rossi-alpha, feynman-alpha and gamma differential die-away concepts as a potential alternative/complement to the traditional thermal neutron based analysis in safeguards," 2015. draft submitted to journal.